ABSTRACT

THEORY AND DESIGN OF MIXED LUMPED-DISTRIBUTED CROSS-COUPLED FILTERS WITH APPLICATIONS TO LINEAR PHASE SHIFTER AND TUNABLE FILTERS

By
Sanghoon Shin

Using cross-coupled networks of a new concept, transmission zeros were efficiently located in the complex frequency-domain. With this approach, the group delay and attenuation slope of the circuit network can be controlled to get both sharp rejection characteristics and linear phase slopes. In order to achieve this performance, various types of combline filters are suggested. Various simulation tools (commercial linear circuit and E-M simulators), as well as the developed pole-zero locator program, were used to design a new class of cross-coupled networks. In particular, the pole-zero locator program can be used to extract an equivalent circuit of the topology that is established from ether EM-simulated data or measured data.

A new cross-coupled quasi-elliptic combline bandpass filter is presented, borrowing the distributed implementation of the capacitance (a top surface metalized dielectric block added as an appliqué to the top of the circuit), which was conventionally used without metalization to enhance the directivity of the microstrip couplers. The required cross coupling value was achieved by changing the substrate thickness, dielectric constant and area of the top surface metallization of the dielectric block. Effectively, an inhomogeneous transmission line was used to achieve source-load direct cross-coupling with at least one additional transmission zero.

The first application presented, is a new type of reflection-type analog phase shifter using tunable short-terminated combline filters (STCL). An asymptotically approached 360-degree total phase shift is obtained, with a large linear range and an insertion loss of less than -1.5 dB over the full phase shift range at 5 GHz. The second approach presented, which is a new concept, is a tunable finite-transmission-zero filter, taking advantage of the unavoidable frequency dependence of each coupling. In order to obtain such a performance, ferroelectric or ferromagnetic stacked substrates are suggested for tuning the extra transmission zeros as well as the center frequency.

THEORY AND DESIGN OF MIXED LUMPED-DISTRIBUTED CROSS-COUPLED FILTERS WITH APPLICATIONS TO LINEAR PHASE SHIFTER AND TUNABLE FILTERS

By
Sanghoon Shin

A Dissertation
Submitted to the Faculty of
New Jersey Institute of Technology
In Partial Fulfillment of the Requirement for the Degree of
Doctor of Philosophy in Electrical Engineering

Department of Electrical Computer Engineering

May 2002

APPROVAL PAGE

THEORY AND DESIGN OF MIXED LUMPED-DISTRIBUTED CROSS-COUPLED FILTERS WITH APPLICATIONS TO LINEAR PHASE SHIFTER AND TUNABLE FILTERS

Sanghoon Shin

5-2-02

Dr. Richard V. Snyder, Dissertation Advisor — Date
Adjunct Professor, Department of Electrical and Computer Engineering, NJIT
RS Microwave Inc.

5/2/02

Dr. Edip Niver, Dissertation Co-Advisor — Date
Associate Professor, Department of Electrical and Computer Engineering, NJIT

5/2/02

Dr. Gerald Whitman, Committee Member — Date
Professor, Department of Electrical and Computer Engineering, NJIT

05/02/2002

Dr. Sridhar Kanamaluru, Committee Member — Date
Sarnoff Corp.

5/2/02

Dr. Aly Fathy, Committee Member — Date
Sarnoff Corp.

BIOGRAPHICAL SKETCH

Author: Sanghoon Shin

Degree: Doctor of Philosophy

Date: May 2002

Date of Birth:

Place of Birth:

Undergraduate and Graduate Education:

- Doctor of Philosophy in Electrical Engineering,
  New Jersey Institute of Technology, Newark, NJ, 2002

- Master of Science in Electrical Engineering,
  Polytechnic University, Brooklyn, New York, 1996

- Bachelor of Science in Polymer Engineering,
  Han-Yang University, Seoul, Korea, 1994

Major: Electrical Engineering

Presentations and Publications

Sanghoon Shin, Richard V. Snyder, and Edip Niver,
"360-degree linear analog phase shifter design using tunable short-circuit terminated combline filters,"
IEEE International Microwave Symposium digest, Volume 1, 2001,
pp. 303 –306, May 2001.

Sanghoon Shin, Richard V. Snyder
"At least N+1 Finite Transmission Zeros Using Frequency Dependent Negative Source-load Coupling,"
IEEE Microwave and Wireless components letters, submitted on March 2002.

Richard V. Snyder, Edip Niver, Keehong Um, and Sanghoon Shin
"Suspended resonators for filters-reduced λg excitation of evanescent cavities using high dielectric constant feeding lines,"
IEEE International Microwave Symposium digest, June 2002.

Richard V. Snyder, Sanghoon Shin, Edip Niver

"Linear Analog Phase Shifter Design Using Quasi-Elliptic Short-circuit Terminated Combline Filters,"

IEEE MTT-Transactions, submitted on March 2001.

To my beloved family

ACKNOWLEDGEMENT

First of all, I would like to express my heartiest thanks and respect to my supervisor Professor Richard V. Snyder, whose stimulating suggestions, excellent guidance, and constant encouragement helped me in all the time of research and writing of this thesis.

I would also like to express my sincere thanks to Professor Edip Niver for providing me with the chance to start my research in NJIT and helping me delve into the various RF/Microwave areas.

I am deeply indebted to Professor Gerald Whitman for all his support, interest and valuable insights for my research as well as my life.

I would also like to thank Dr. Sridhar Kanamaluru and Dr. Aly Fathy for their professional guidance, detailed comments on the drafts of this thesis and insightful suggestions for my future work.

I would like to thank Nayoung, my sister-in-law, who looked closely at the final version of the thesis for English style and grammar, correcting both and offering suggestions for improvement.

Especially, I must acknowledge my parents who have always been there for me in great need. Their immeasurable devotion and encouragement gave me strength to push through difficulties. I would also like to give my special thanks to my son, Seungyong, my daughter, Sangah and my parents-in-law for their strong love and constant support.

Finally, this thesis is dedicated to my wife, Jeoungyeon whose patient love and ceaseless encouragement enabled me complete this work.

TABLE OF CONTENTS

TABLE OF CONTENTS
(Continued)

Chapter **Page**

LIST OF TABLES

LIST OF FIGURES

LIST OF FIGURES
(Continued)

Figure **Page**

LIST OF FIGURES
(Continued)

LIST OF FIGURES
(Continued)

CHAPTER 1

COMBLINE FILTER DESIGN AND ANALYSIS USING NEW CROSS-COUPLED NETWORK

1.1 Objective

The objective of this dissertation is to present a new analysis and synthesis method which is applicable to various RF/Microwave applications. As result of applying this method, a new type of cross coupling network is presented to control the magnitude and phase characteristics of the filters used in these applications. The new network is applied to a wide-band linear phase shifter as well as microwave filters with tunable center frequencies and tunable transmission zeros.

1.2 Introduction

Combline filters are among the most popular microwave filters because of the simplicity of construction, convenient tunability and small sizes. Non-adjacent cross couplings give a number of alternative paths along which a signal may propagate between the input and output ports. Depending on the phasing of the signals, the mulitpath effect may produce finite transmission zeros on the real frequency axis (imaginary axis) or on the imaginary frequency axis (real axis), which makes group delay flattening [1].

In order to obtain such performance, this chapter introduces several types of quasi-elliptic combline filters. First, the open-circuited combline filter with negative coupling effects is proposed. By means of using the negative coupling, finite transmission zeros can be produced. As for the phase shifter application, a short circuit terminated combline is presented as a modification of the open-circuited combline filter. A dielectric overlay "brick" is used to enhance this negative coupling effect. Finally, a source-load coupled

quasi-elliptic filter that employs the inhomogeneous-coupled transmission line coupler is presented. Regarding the source-load direct coupling, very low coupling is realizable by using this transmission line directional coupler. In order to plot poles and zeros for the given topology, a pole-zero locator program was developed.

1.3 Nodal Admittance Matrix Method (Pole-zero locator)

A presented circuit analysis program capable of both symbolic and numeric calculations is proposed. Most commercial simulator programs designed for circuit analysis perform only numerical analysis. Since symbolic analysis derives equations instead of numbers, it can be inferred how certain components affect the yield, flatness, sensitivity, poles, and zeros of the circuit, which are designed in this chapter.

The nodal admittance matrix method is frequently used for the computer-aided analysis of linear circuits in the frequency domain. Once one of the principle nodes is selected as the reference node, equations based on KCL (Kirchhoff's Current Law) are written at the other principal nodes. A voltage is assigned at each of node. The voltages V_N of all nodes are assumed as unknowns [2]. It is assumed that an independent current source of one ampere has been connected between node 1 and the reference node. The equations are set up in the form of a matrix expression

$$YV_N = I_N = \begin{bmatrix} 1 \\ 0 \\ 0 \\ \vdots \\ 0 \end{bmatrix} \tag{1.1}$$

where

Y = a square nodal admittance matrix (a degree of this matrix equals the number of the nodes in the analyzed circuit)

V_N = a vector of node voltages taken with respect to a point outside the circuit

I_N = a vector of terminal currents of the independent current sources connected between the nodes and the reference node of the circuit

The solution of the nodal matrix expression (1.1) provides all node voltage values of a circuit.

When a circuit as shown in Figure 1 is taken into account, the circuit equations are derived from the application of the Kirchoff's current law to each node of circuit.

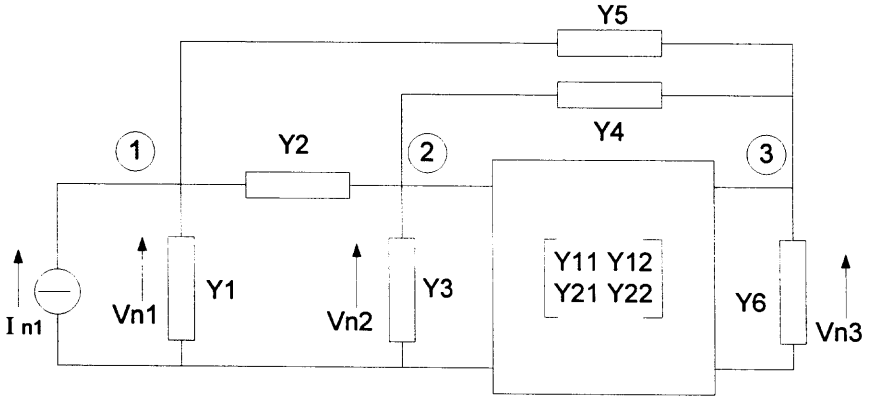

Figure1.1 A circuit to illustrate the principles of the formulation of the nodal voltage equations.

Node 1:

$$Y_1V_{N1} + Y_2(V_{N1}-V_{N2}) + Y_5(V_{N1}-V_{N3}) = I_{N1}$$

Node 2:

$$Y_3V_{N2} + Y_2(V_{N2}-V_{N1}) + Y_4(V_{N2}-V_{N3}) + y_{11}V_{N2} + y_{12}V_{N3} = 0$$

Node 3:

$$Y_6V_{N3} + Y_2(V_{N3}-V_{N2}) + Y5(V_{N3}-V_{N1}) + y_{21}V_{N2} + y_{22}V_{N3} = 0$$

These equations can be written in the matrix form as below:

$$\begin{bmatrix} Y_1+Y_2+Y_5 & -Y_2 & -Y_5 \\ -Y_2 & Y_2+Y_3+Y_4+y_{11} & -Y_4+Y_{12} \\ -Y_5 & -Y_4+Y_{21} & Y_4+Y_5+Y_6+y_{22} \end{bmatrix} \begin{bmatrix} V_{N1} \\ V_{N2} \\ V_{N3} \end{bmatrix} = \begin{bmatrix} I_{N1} \\ 0 \\ 0 \end{bmatrix}$$

The nodal admittance matrix of a circuit is derived using the rules as follows:

(1) Admittance Y: a passive admittance connected between nodes i and j contributes a term into the nodal admittance matrix given by

$$\begin{array}{c} \\ \\ \text{row} \end{array} \begin{array}{c} \\ \text{(i)} \\ \text{(j)} \end{array} \begin{array}{c} \text{column} \\ \begin{bmatrix} \\ \cdots \\ \\ \cdots \\ \\ \end{bmatrix} \end{array} \begin{array}{c} \\ \text{(i)} \\ \text{(j)} \end{array} \begin{bmatrix} \vdots & & \vdots & \\ \cdots & Y & \cdots & -Y & \cdots \\ \vdots & & & & \\ \cdots & -Y & \cdots & Y & \cdots \\ \vdots & & \vdots & & \end{bmatrix}$$

(2) If node i is the reference node, then the admittance Y appears only on the main diagonal of the Y matrix in the element Y_{ii}:

$$\begin{array}{c} \\ \text{(i)} \end{array} \begin{array}{c} \text{(i)} \\ \begin{bmatrix} \\ \cdots \\ \\ \end{bmatrix} \end{array} \begin{bmatrix} \vdots & \\ \cdots & Y & \cdots \\ \vdots & \end{bmatrix}$$

The transfer function H(jω) is calculated by multiplying the inverse of the admittance matrix to the current column vector. The output voltage V_k at the load node to the input current I_1 of the independent source is the voltage transfer function:

$$H(jw)=V_k=Y^{-1}I=|H(jw)|e^{j\phi(w)} \tag{1.2}$$

Poles and zeros can be calculated from the numerator and denominator polynomials with the root find routine from the equation (1.2) by using MatLab's symbolic library. Input data format has SPICE circuit simulator input data format (Table 1.1). However, this program only calculates the poles and zeros for the RLC equivalent circuit of the given topology. Thus, this approach cannot be applied to the distributed circuit at this stage. Simulated results will be shown in following sections respectively. Insertion loss frequently calculated in filter design is obtained as follows:

$$IL = -20\log(|Y_s + Y_L| \cdot |H(jw)|) \tag{1.3}$$

Reflection coefficient and return loss are determined by

$$\Gamma_{in} = \frac{Y_{in} - Y_s}{Y_{in} + Y_s} = 1 - 2\frac{V_1}{I_1}Y_s \tag{1.4}$$

$$RL = -20\log|\Gamma| \quad , \quad dB \tag{1.5}$$

Table 1.1 Input Data Example of a Two-pole Cross-coupled Bandpass Filter for Pole-zero locator program

```
RES 1 0 50  0
CAP 1 2 0.91e-12 0
PLC 2 0 0.32273e-9 2.34123e-12
IND 2 3 5.27e-9 0
PLC 3 0 0.32273e-9 2.34123e-12
CAP 3 4 0.982e-12 0
CAP 1 4 0.816e-12 0
RES 4 0 50 0
```

1.4 Conventional Two-pole Combline Filter

A conventional two-pole combline filter with capacitive transformers is illustrated in Figure 1.2 (a). The combline filter is composed of commensurate parallel-coupled lines. Each line is short-circuited to the ground at the same end, whereas the opposite ends are terminated in lumped capacitors. The line length of the combline filter cannot have an electric length of ninety-degree. Such being the case, the electric and magnetic field will cancel each other, generating zero coupling. The line length is typically 45 degrees at the resonance frequency, but can range from 10 to 88 degrees. Thus, combline filter is physically compact and has a broad stopband bandwidth [3][4][5].

The equivalent circuit of the combline filter is shown in Figure1.2 (b). The shunt resonators are formed by the inductive reactance of the shunt SC stubs in parallel with lumped capacitors at the resonator open-ends. Coupling between the adjacent lines is provided through electromagnetic fields in the gap between them. In this case, the magnetic coupling is predominant, as the magnetic and electric couplings are not equal. Therefore, the coupling between the adjacent lines can be treated as series lumped inductors in the equivalent circuit.

The separation between adjacent lines sets the strength of coupling. The electric field distribution of adjacent coupled line is illustrated in Figure 1.2 (a) by using Agilent HFSS EM simulator. Figure 1.2 (c) shows the insertion, return, and group delay response using a commercial circuit simulator. Pole-zeros of the equivalent circuit from the pole-zero locator program are shown in Figure1.2 (d).

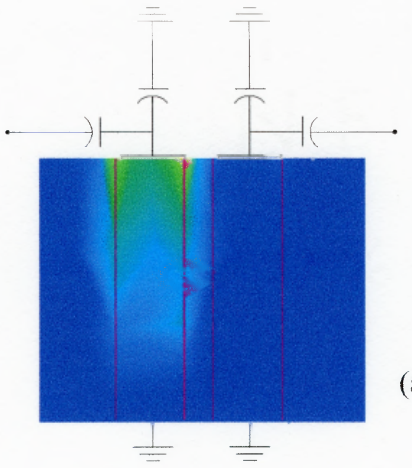

(a)

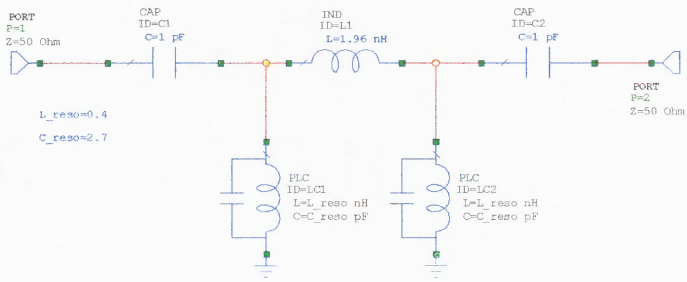

(b)

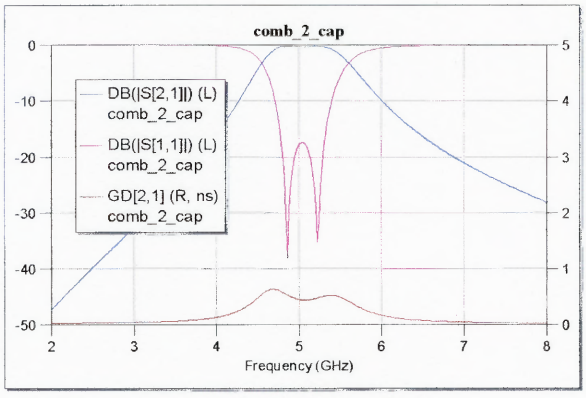

(c)

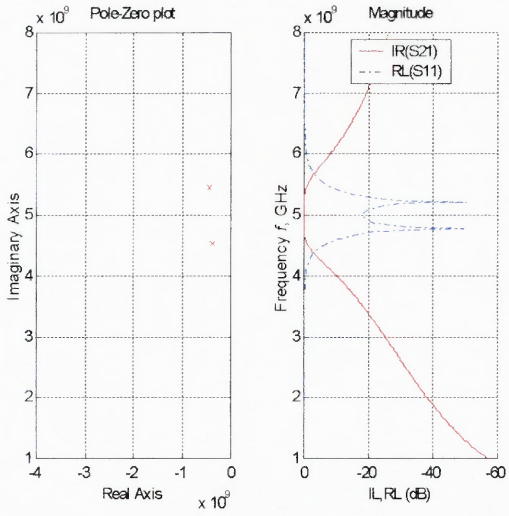

(d)

zeros =

0
0
0

poles =

1.0e+009 *

-0.4298 + 5.4618i
-0.4298 - 5.4618i
-0.3794 + 4.5360i

Figure 1.2 A conventional two-pole combline filter with capacitive input-output coupling circuits; (a) Electric field distribution and diagram, (b) Equivalent circuit, (c) Circuit simulation result (S-parameters and group delay), (d) Pole-zero and magnitude response to the equivalent circuit from the pole-zero locator program. (Zeros and imaginary conjugate poles are not displayed due to the frequency scale).

1.5 Open-circuited Combline Filter

It has been the case that the conventional combline filter uses short circuit-terminated parallel-coupled lines (PCL). However, in the new approach, open-circuited ends of the transmission line resonators are connected directly to input-output coupling networks (Figure 1.3 (a)).

The propagation velocities of the TEM even and odd modes in microstrip parallel–coupled lines are not equal [6]. The open-circuited section reduces the odd-mode characteristic impedance of the parallel-coupled line and introduces the negative coupling. The negative coupling (due to the parasitic bridging capacitive coupling at this high E-field region of the open-circuited PCL) can be utilized to implement either a single or a pair of real-frequency transmission zeros near the filter passband [6].

EM-field distribution explicitly shows strong electric fields at the end of closely spaced open-circuited coupled line as in Figure 1.3 (b). Using only the parasitic capacitance naturally present in the parallel-coupled lines, single transmission zero resulting from the equivalent series tank circuit is obtained. Figure 1.3 shows the equivalent circuit, S-parameter response, pole-zero location of the equivalent circuit, and field distribution, respectively. Figure 1.4 shows the 3-D EM simulation result of the open-circuited two-pole combline filter.

Contrary to the circuit simulator results, EM simulation result shows two transmission zeros. The extra coupling between the bends, which is not a part of the parallel-coupled lines, makes another transmission zero, which was not attainable in the circuit simulation result.

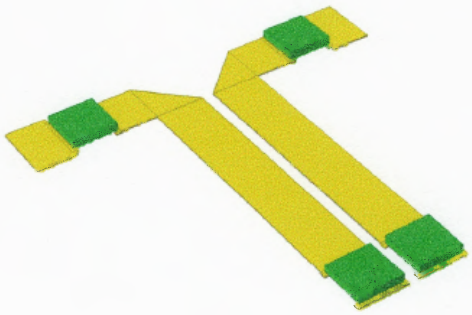

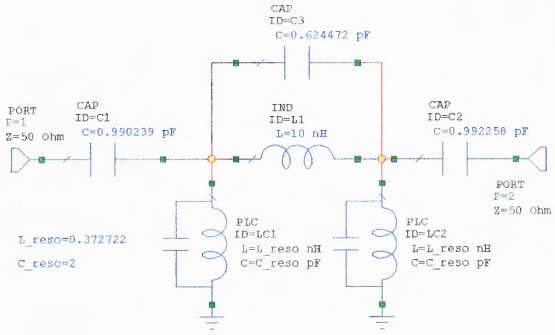

(a)

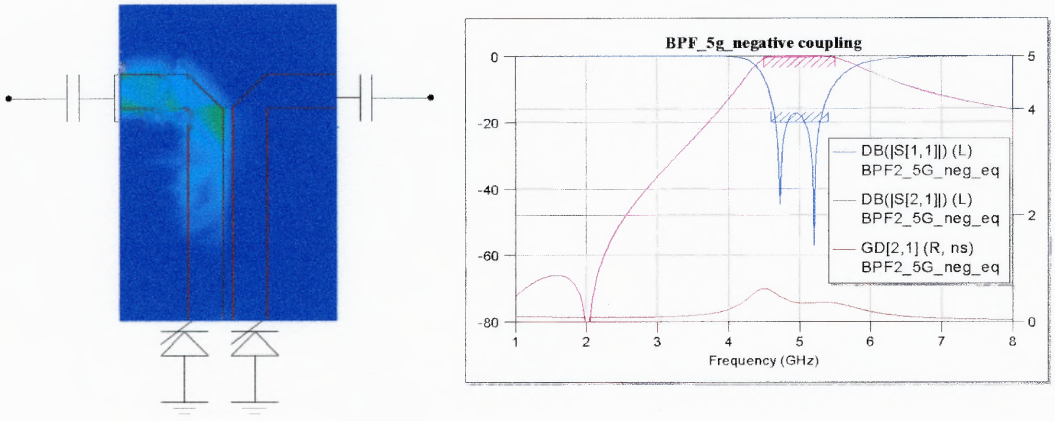

(b)

Figure 1.3 Open-circuited parallel coupled line two-pole combline filter with capacitive input-output coupling circuits; (a) Diagram and equivalent circuit, (b) Electric field distribution using HFSS and S-parameter response using commercial circuit simulation result.

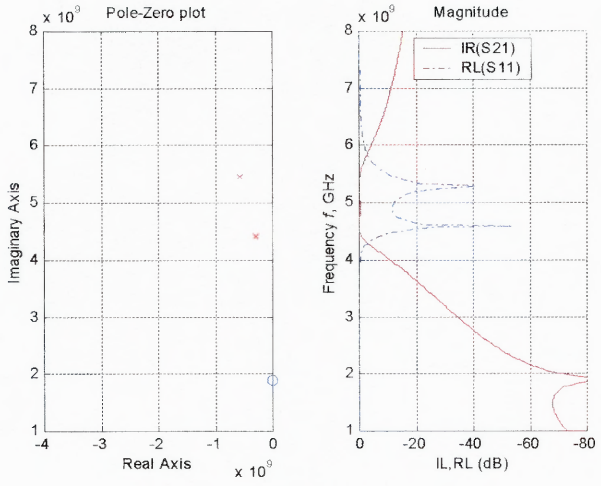

(c)

zeros =
1.0e+009 *
0
0
0
0 + 1.9001i
0 - 1.9001i

poles =
1.0e+009 *
-0.6004 + 5.8815i
-0.6004 - 5.8815i
-0.3124 + 4.7192i
-0.3124 - 4.7192i
-3.5739
-3.4937

Figure 1.3 Open-circuited parallel coupled line two-pole combline filter with capacitive input-output coupling circuits; (c) Pole-zero and magnitude response to the equivalent circuit from the pole-zero locator program (continued).

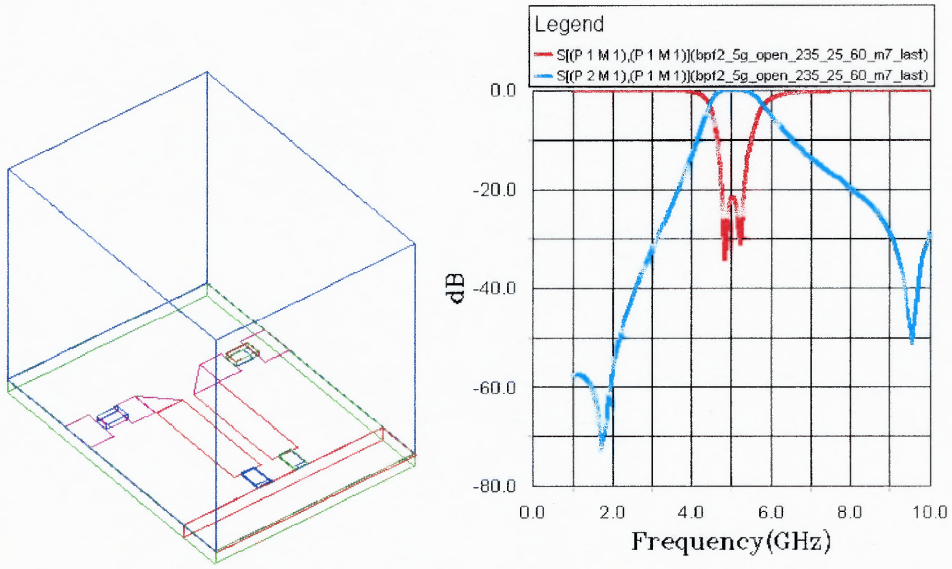

Figure 1.4 Full 3-D EM simulation result of the open-circuited two-pole combline filter.

A conductor wall between bends is inserted to see the extra path from source to load coupling (Figure 1.5). The length of a conductor wall (Electrical wall) gradually increased from bends towards tuning capacitors between the PCL section. It moves the upper TZ to the right. However, the conductor wall did not completely block the source to load extra coupling. As conductor wall increases, the upper TZ eventually disappeared. However, the left TZ still exists.

Techniques to equalize the mode velocities on microstrip coupler characteristics have been reported by placing an additional coupling dielectric bar along the gap between the parallel-coupled lines [7]. When a dielectric overlay structure is used over the parallel coupled-line filter, transmission zeros can be controlled. Figure 1.6 shows that the transmission zero on the right is moved to the passband region after adding a dielectric brick ($\varepsilon_r = 5$, thickness = 10 mils).

It is well known that at most N-2 finite transmission zeros can be produced out of N-resonators without source-load coupling[1]. This means there should be an extra coupling beyond resonators. In this two-pole open-circuited filter case, source to load coupling path exists between bends. Thus, putting a dielectic "brick" into the circuit to enhance the negative coupling between PCL sections is by no means advisable for the two-pole open-circuited case (Actually there might me 3 TZs). Since this open-circuited structure has already an embedded source to load coupling, the negative coupling cannot

[1] Smain Amari, "Direct synthesis of Folded symmetric Resonator filters with source-Load coupling", IEEE Microwave and wireless components letter Vol.11 No.6 June 2001.

be exclusively enhanced. In order to use a negative coupling only or source-load coupling, higher order filters or conventional combline filters should be utilized.

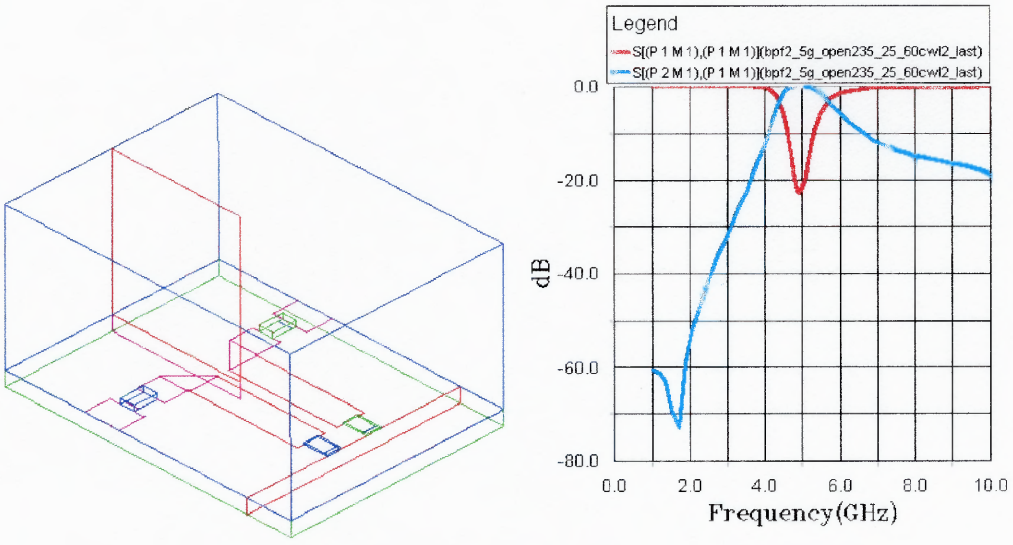

(a) After inserting a conductor wall up to bends.

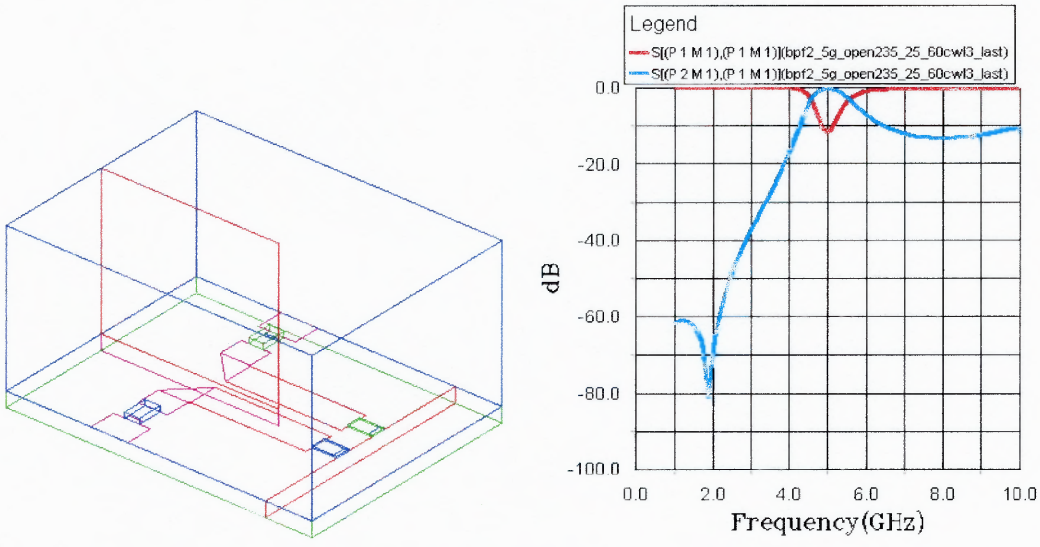

(b) After increasing the conductor wall length toward tuning capacitors(i).

Figure 1.5 Extra path between the bends.

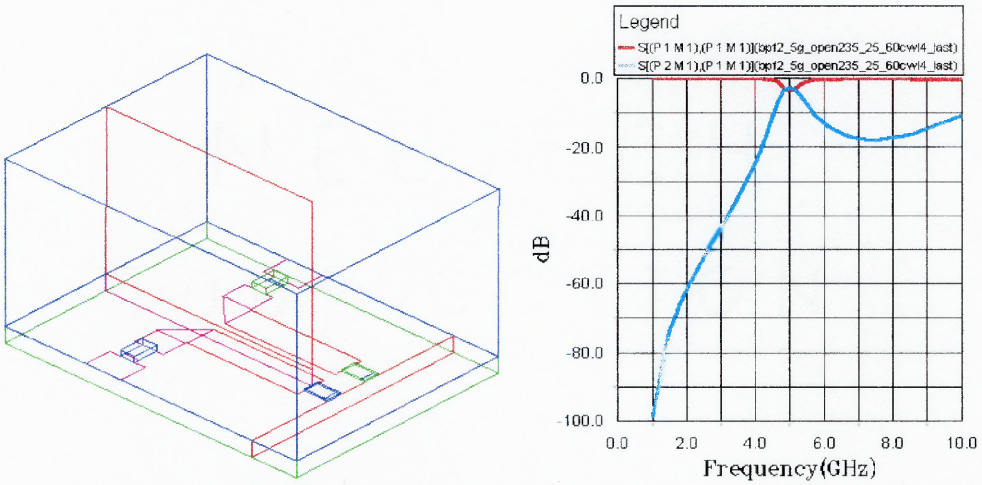

(c) After increasing the conductor wall length toward tuning capacitors(ii).

Figure 1.5 Extra path between the bends (continued).

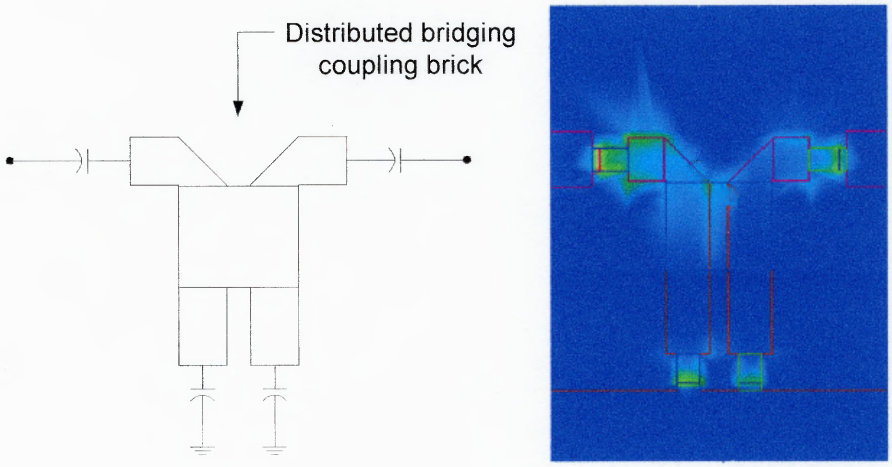

E-field
distribution
at 5 GHz

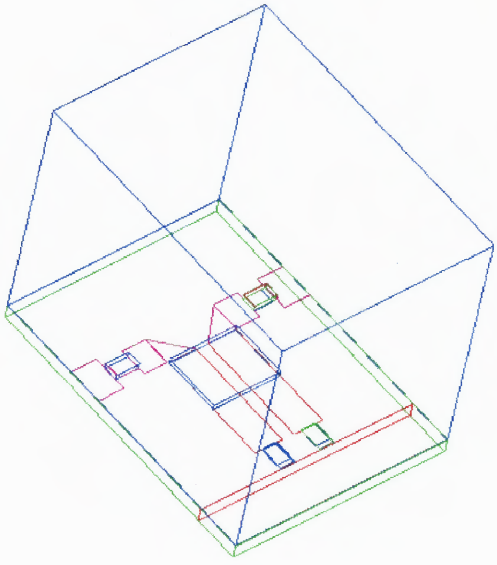

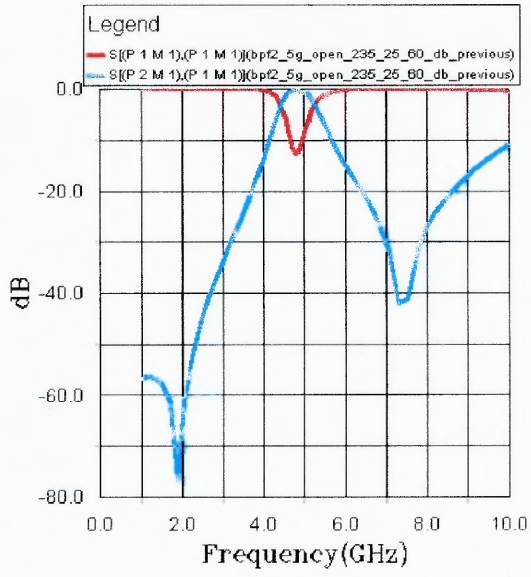

Figure 1.6 Open-circuited two-pole combline filter simulated response using HFSS with a dielectric brick overlay (ε_r=5, h=10mils) as a coupling device.

1.5.1 Relocated Tuning Capacitors

Tuning capacitors (as shown in Figure 1.3 (a)) are located in a high H-field area. This is not the proper position to use the tuning capacitance effectively. When tuning capacitors are moved to the opposite ends of the parallel-coupling lines, extra transmission zeros of the filter can be controlled more effectively.

In Figure 1.8, a dielectric brick is located on the bends, not on the PCL section. The reason is to use the embedded source to load coupling effectively without affecting main PCL coupling. To make narrow bandwidth filter (here, BW=200MHz), line gap between PCL is increased. Although a negative coupling effect is reduced, two TZs are closer to the center frequency than the original open-circuited case. Simulation result shows two TZs with keeping center frequency at 5 GHz as shown in Figure 1.8.

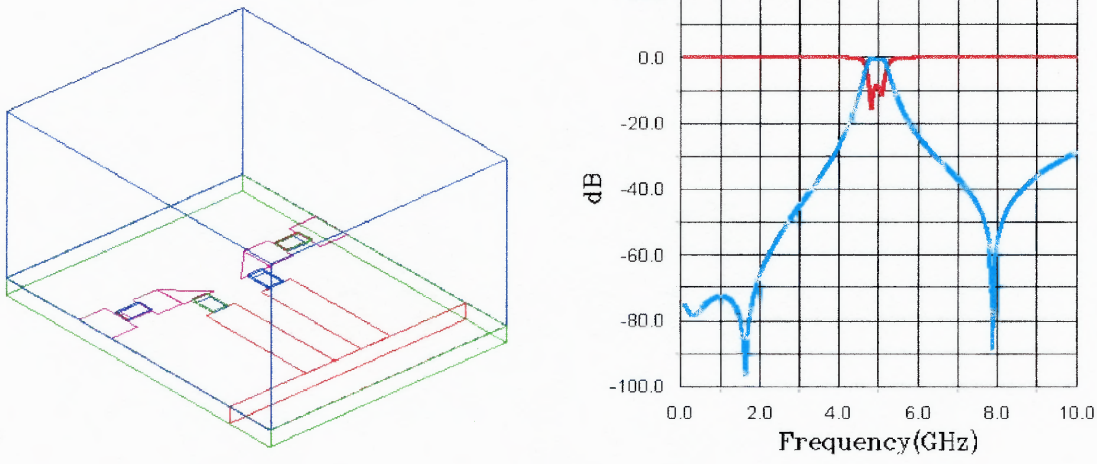

Figure 1.7 Relocated tuning capacitors at high e-field region (open-circuited combline filter, Fc= 5GHz, BW=300MHz).

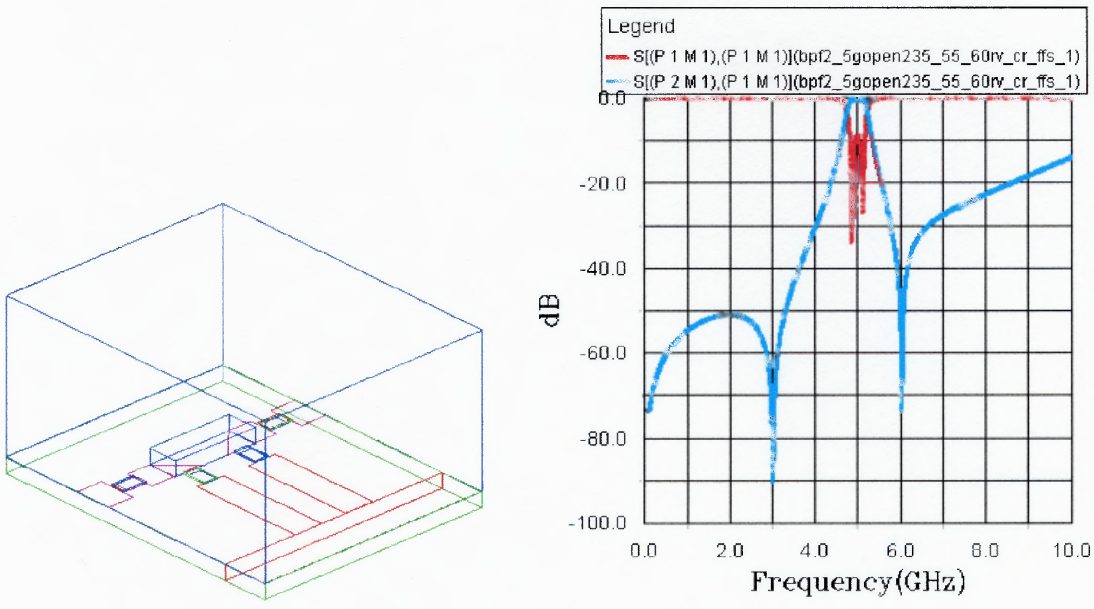

Figure 1.8 Dielectric brick (Er=20, h=20 mils) is located to enhance the source-load coupling (Center frequency 5GHz is still kept).

1.6 Short-circuit terminated combline filter (SCTL filter)

Usually filters are used as frequency magnitude selective devices (two port devices). When the output port of the filter is short circuit terminated (one port device), signals pass once through the filter, and then reflect from the short circuit termination (Figure 1.9). This reflected signals pass through the filter again. At this time, the phase shift of the reflected signal is almost twice the insertion phase. When this approach is applied to the reflection-type analog phase shifter design, the overall phase shift range is larger and linear than the conventional L-C series-resonance type design. This application will be discussed in Chapter 2 in detail. Figure 1.9 (a) shows the SCTL filter diagram, electric field distribution and an equivalent circuit.

To actually see the response of the STCL filter, the filter is simulated with a terminating resistance of slightly greater than zero ohm. This allows for viewing the

shape of the loss curve, which otherwise would be flatter. Pole-zero plot is shown in Figure1.9 (c). To utilize the phase doubling effects for the phase shifter, varactor diodes are used at lumped capacitor locations to tune the filters as shown in Figure 1.9(d). Magnitude response and phase response is shown in Figure1.9 (d). The doubled reflection phase response is clearly shown in Figure1-9 (d).

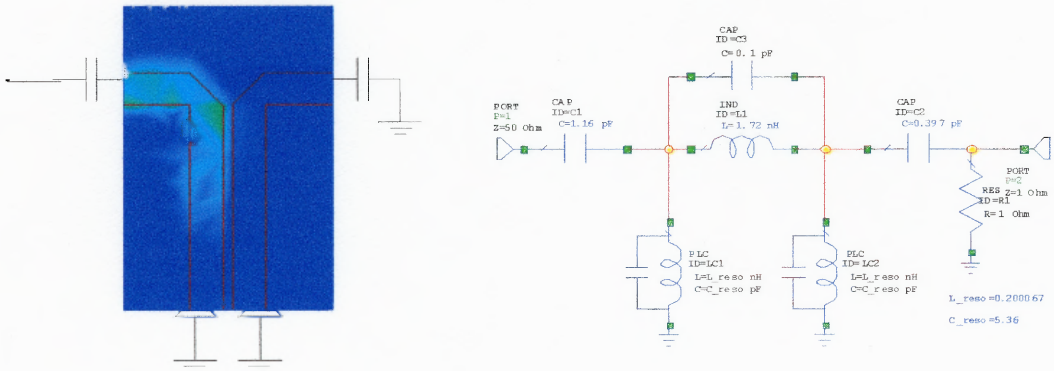

(a)

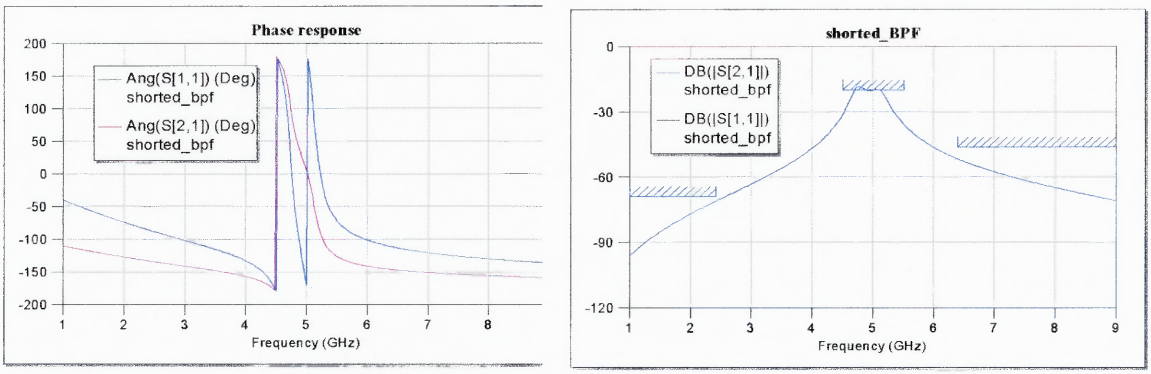

(b)

Figure 1.9 Short circuit–terminated open-circuited combline filter; (a) Diagram and equivalent circuit, (b) Magnitude and phase responses using commercial circuit simulator.

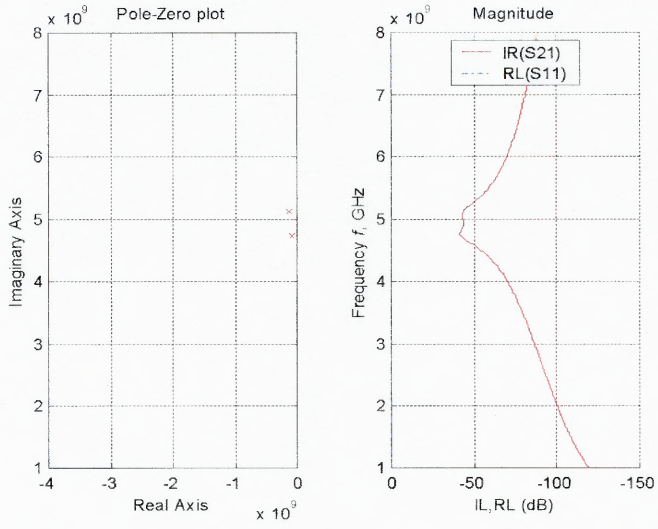

zeros =

1.0e+010 *

0

0

0

0 + 1.2135i

0 - 1.2135i

poles =

1.0e+011 *

-8.6010

-0.0012 + 0.0512i

-0.0012 - 0.0512i

(c)

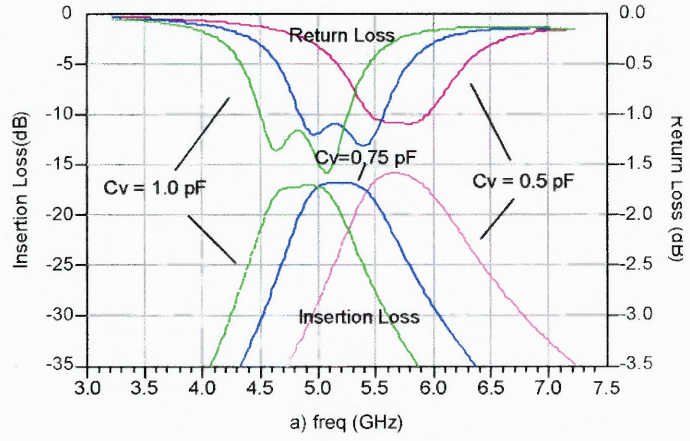

(d)

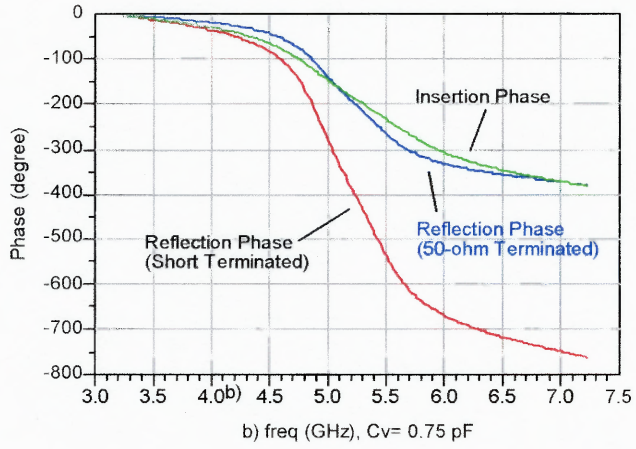

Figure 1.9 Short circuit–terminated open-circuited combline filter; (c) Pole-zero plot using pole-zero locator program, (d) Tunable SCTL filter response when varactor diodes are use(continued).

1.7 Source-load Direct Coupling

For mobile communications or satellite systems, microwave filters should have a constant group delay and a high rejection slope out of band. Discrete transmission zeros (where the S_{21} goes to zero) can be obtained in the filter stopband by adding cross coupling (coupling between non-adjacent resonators). In planar circuit design, cascaded triplet or quadruplet filters have been used for making finite transmission zeros [8][9].

In this section, by adding an extra path to the source-load rather than to non-adjacent resonators, finite transmission zeros are achieved. A new type of source-load coupling two-pole combline filter is illustrated in Figure1.10 (a). The number of resonators that the coupling "skips over" will determine the characteristics of the transmission zeros. Skipping over an even number of resonators results in a symmetric frequency response, with a zero on the both side of the passband [10]. Figure 1.10 (b) shows the equivalent circuit of the two-pole bandpass filter with a source-load capacitive coupling and frequency response to the equivalent circuit. Two finite transmission zeros are shown clearly on the real frequency axis in Figure 1.11 by using the pole-zero locator program.

A dielectric "brick", metalized on the top surface only, (effectively an inhomogeneous transmission line) is used to give the source-load coupling as shown in Figure 1.10(a). The advantage of this design is that the required cross coupling value is realized by changing the substrate thickness, dielectric brick constant of the brick, or top metal size of the transmission "brick". Connection wire side effects (lead inductance) can be avoided. Calculation for the overlapping conductor size of the cross-coupled transmission line block is determined by parallel plate capacitance formula.

$$C = \frac{A\varepsilon_r\varepsilon_o}{d} \tag{1.6}$$

where A is the area of top and bottom overlapped conductor area,

d is the distance between conductors.

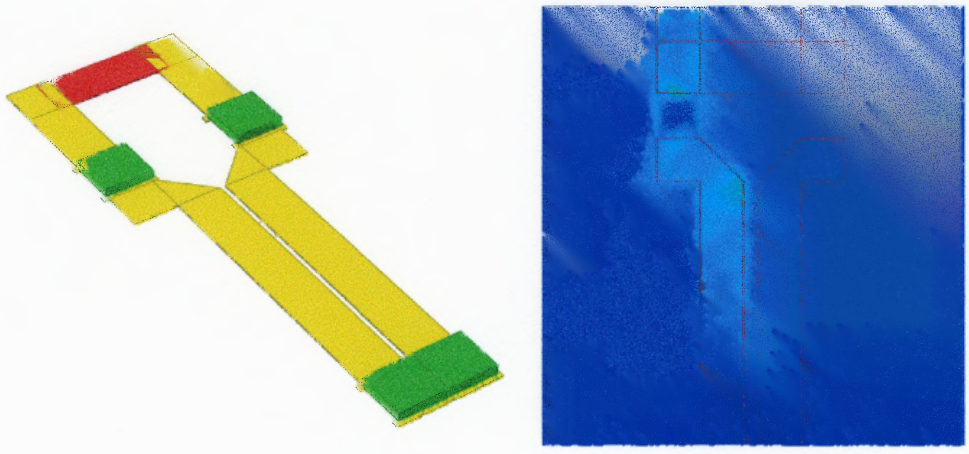

(a)

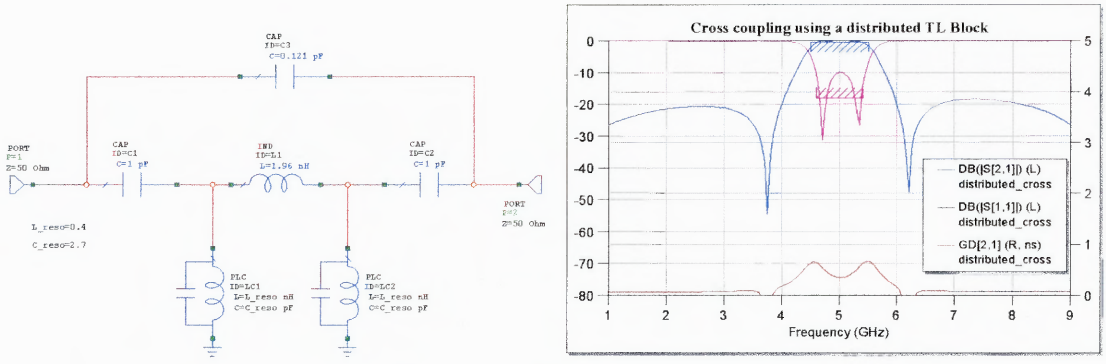

(b)

Figure 1.10 Source-load cross coupled two-pole combline filter; (a) Diagram and EM field distribution, (b) Circuit simulation result to the equivalent circuit.

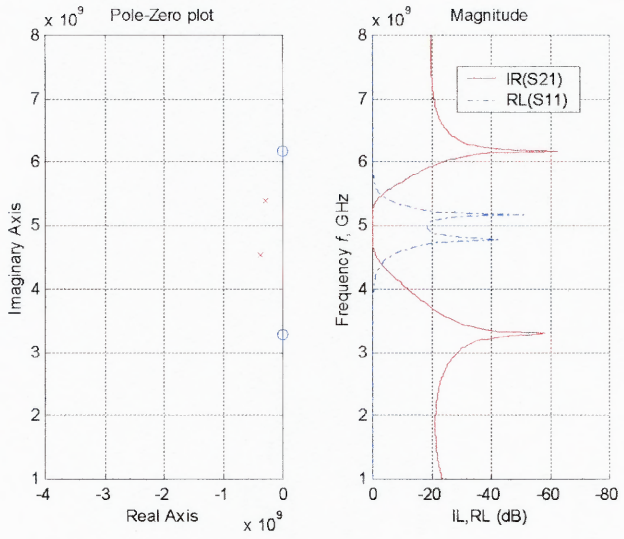

zeros =
1.0e+009 *
0
0 + 6.1828i
0 - 6.1828i
0 + 3.2849i
0 - 3.2849i

poles =
1.0e+009 *
-0.2882 + 5.4005i
-0.2882 - 5.4005i
-0.3794 + 4.5360i
-0.3794 - 4.5360i

Figure 1.11 Pole-zero plot for the equivalent circuit of source-load coupled two-pole combline filter (continued).

Figure 1.12 shows the magnitude yield analysis by changing the thickness of the substrate of transmission line coupler to obtain the same capacitance as a design parameter. Microstrip coupler directivity comparison with changing the substrate thickness is show in Figure 1.13. A simulated response of the four-pole open-circuited parallel-coupled combline filter with the source-load cross coupling network is displayed in Figure 1.14.

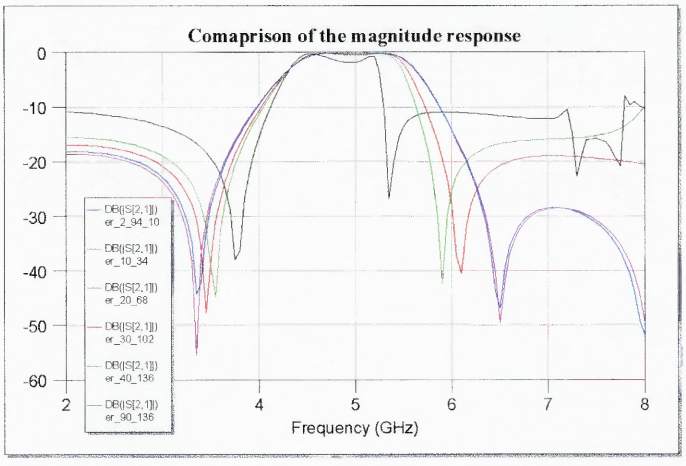

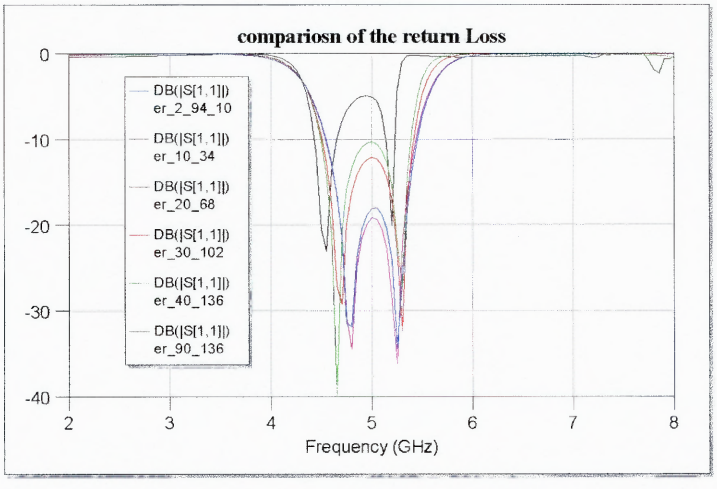

Figure 1.12 Comparison of the magnitude response by changing the thickness of the coupling block substrate.

Table 1.2 Substrate Thickness of The Coupling Brick To Obtain Same Capacitance (C = 0.24 pF) in Figure 1.13

(a) εr = 2.94	H = 10 mils
(b) εr = 10	H = 34 mils
(c) εr = 20	H = 68 mils
(d) εr = 30	H = 102 mils
(e) εr = 40	H = 136 mils

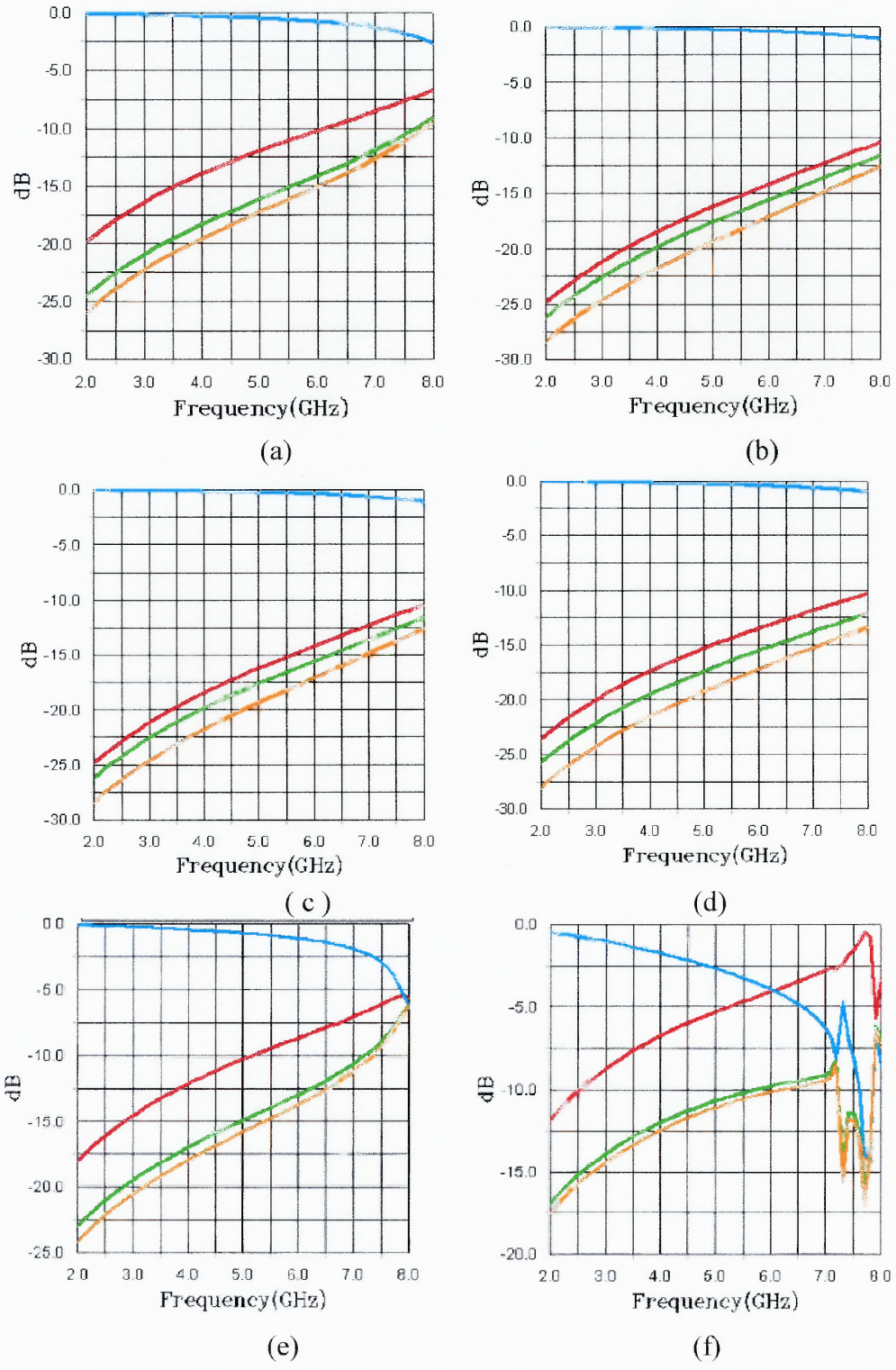

Figure 1.13 Microstrip coupler directivity comparison by changing the substrate thickness as shown in table 1.2.

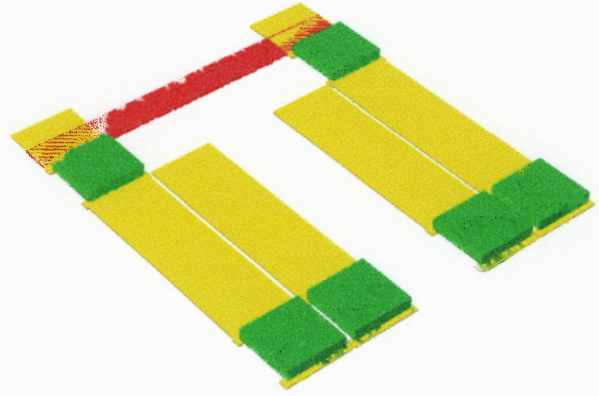

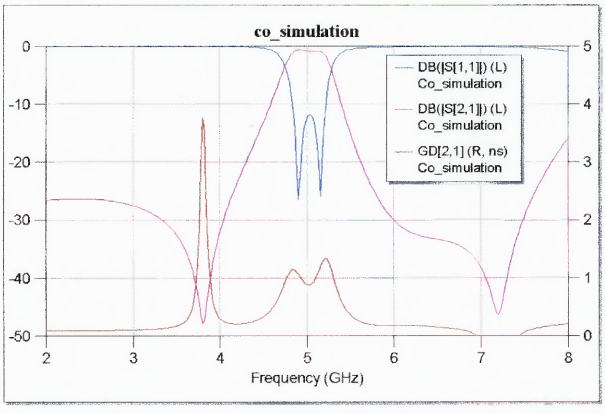

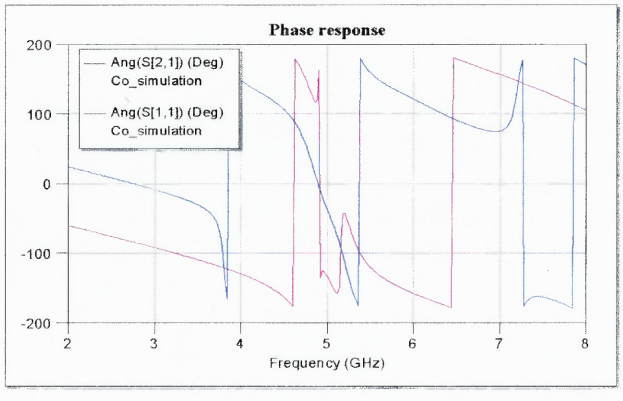

Figure 1.14 The simulated responses of the four-pole open-circuited parallel-coupled combline filter with a source-load cross coupling network.

1.8 E-M Pole-zero Extraction

Poles and zeros location can be extracted from the measured data or from the simulated EM results. The solution of the denominator polynomial of the transfer function (S_{21}) is the same as the solution of the reflection coefficient (S_{11}). Impedance information (Z_{11} and Z_{21}) can be used to find the poles location instead of s-parameter response. Two-pole tapped combline filter is illustrated in Figure 1.15 as an example. This filter is simulated over 4.1GHz 4.5 GHz with 101 discrete points with 3-D EM simulator. The peak point of the impedance plot (Figure 1.16) shows the pole locations of the filter, since transfer function (S_{21}) and input impedance(Z_{11}) have peak values at pole locations.

The extracted poles and zeros locations can be used to verify the equivalent circuit of the distributed filter, such as transmission line or dielectric brick coupling. If poles and zeros locations are matched, the equivalent circuit can be valid for the limited bandwidth. In this example, two pole locations are extracted from the impedance plot. Table 1.3 shows pole location in magnitude and phase format.

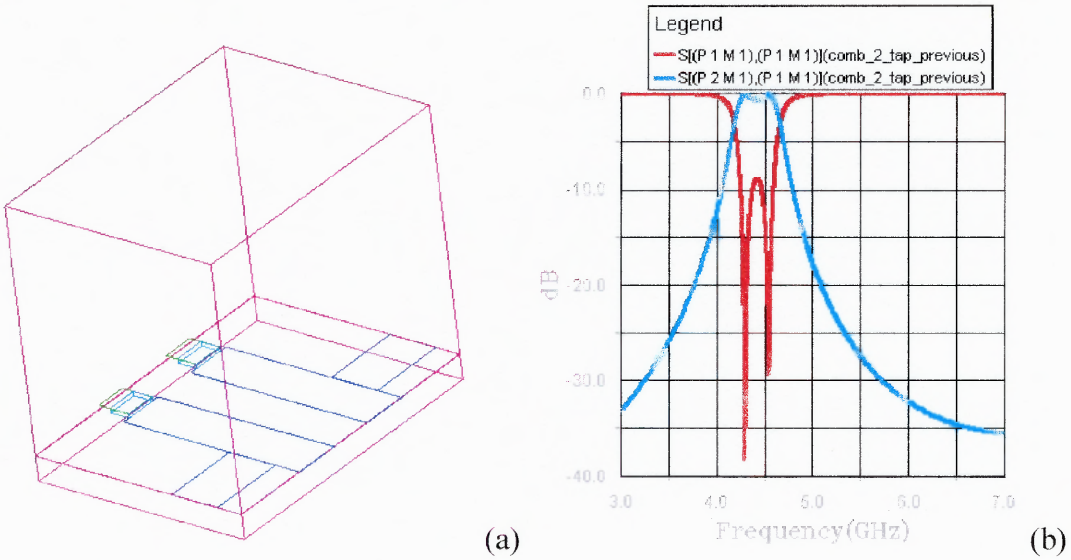

Figure 1.15 Two-pole tapped combline filter; (a) Geometry, (b) Filter response.

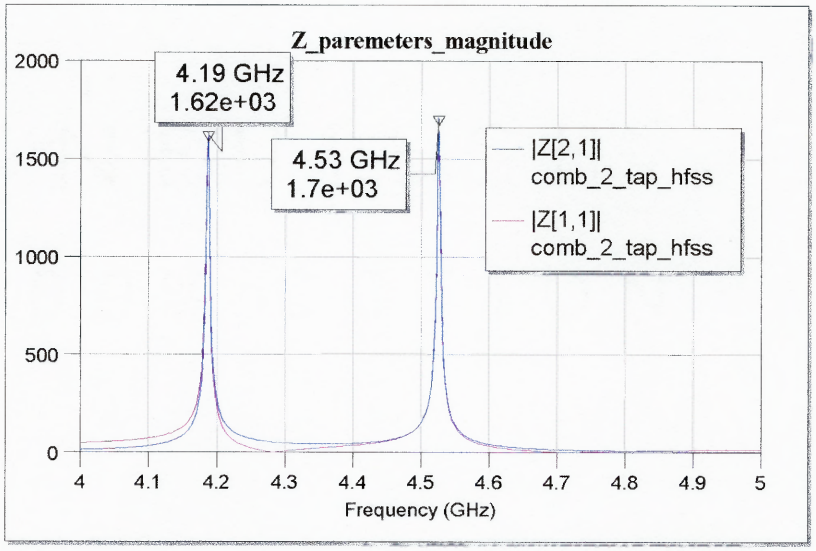

(a)

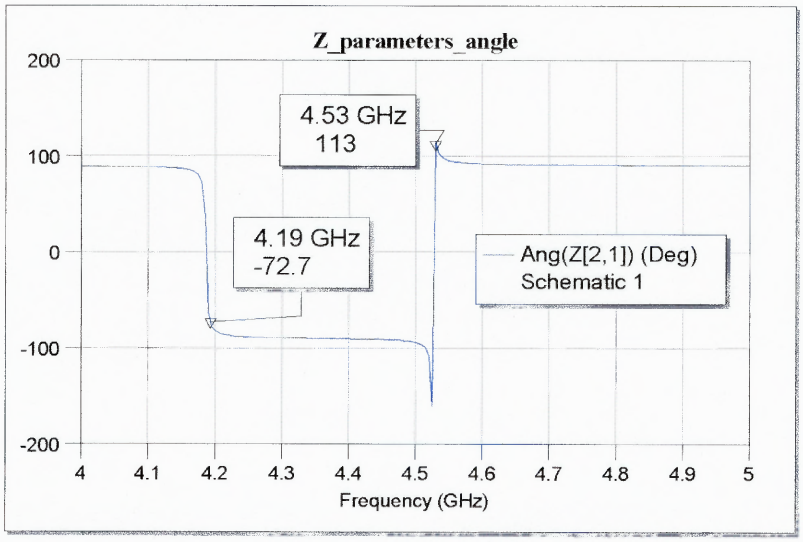

(b)

Figure 1.16 Impedance plot of the two-pole tapped combline filte; (a) magnitude response, (b) Phase plot.

Table 1.3 Impedance Magnitude and Angle of Possible Pole Locations; 4.19 GHz and 4.53GHz

Frequency (GHz)	Z[2,1]	Z[2,1]	Z[1,1]	Z[1,1]
	Schematic 1	Schematic 1	Schematic 1	Schematic 1
	(Mag)	(Ang:Deg)	(Mag)	(Ang:Deg)
4.15	86.245	86.779	129.09	87.755
4.17	201.22	83.186	247.58	84.319
4.175	291.45	80.368	339.82	81.548
4.18	511.3	73.407	563.65	74.64
4.185	1470.8	37.011	1529.1	38.302
4.19	876.03	-62.487	856.66	-61.132
4.195	409.01	-77.92	375.05	-76.495
4.2	266.05	-82.417	227.98	-80.913
4.205	198.39	-84.532	158.27	-82.939
4.21	159.14	-85.76	117.7	-84.065
4.515	345.02	-100.36	340.7	79.708
4.52	613.26	-109.24	603.44	70.85
4.525	1708.9	-161.11	1673.8	19.012
4.53	753.34	115.42	733.6	-64.433
4.535	371.74	102.58	359.5	-77.245
4.54	241.89	98.374	232.04	-81.424

1.9 Conclusions

Quasi-elliptic combline filters with the new type of cross-coupled network were considered. The response of each filter was presented by using circuit, full E-M simulator, and pole-zero locator program. An open-circuit PCL combline filter has shown the negative coupling effect which could not be available in the conventional combline filter. A distributed top-metalized transmission line coupler has been used to implement the source-load direct coupling. In chapter two, a reflection type analog phase shifter with a short circuit terminated combline filter will be discussed as a filter application.

CHAPTER 2

LINEAR ANALOG PHASE SHIFTER DESIGN USING THE SHORT-CIRCUIT TERMINATED COMBLINE FILTER

2.1 Introduction

Analog and digital phase shifters each have certain advantages: the digital device offers accuracy for any bit, but it requires a multiplicity of devices and considerable circuit area to combine enough bits to achieve large phase shift adjustment range. Thus, size, insertion loss, control complexity, and power consumption are significant disadvantages of the digital technique. The analog phase shifter uses less area, and it can achieve large amounts of phase shift with less insertion loss, at the cost of less accuracy and potential temperature sensitivity.

The new technique proposed herein increases the available phase shift range, while reduces the insertion loss and provides for easy temperature compensation [11] through the use of a well-known combline structure in a reflection configuration to provide phase shift based on the reflection phase characteristics of the combline network. Analog phase shifters typically employ matched pairs of tunable L-C series resonant networks in conjunction with 90-degree hybrid couplers, thereby achieving variable phase shift [12]. The signals reflected from the identical diode terminations add up at the isolated port and cancel out at the input port. The performance depends on the isolation, diode termination, coupling balance, etc. At low frequencies, 180-degree phase shift can be achieved if more than one L-C network is employed at each hybrid port, while 180-degree phase shift is asymptotically approached with single L-C sections.

When more phase shift is desired, several identical stages can be cascaded. The available phase shift range for this class of network depends on the capacitance range of the varactor diode, as well as the choice of inductance. To achieve more linear phase shift (vs. frequency), the use of an impedance matching network in front of the varactor diode is more effective than using L-C series resonant network [13],[14]. From a filter point of view, these reactive loads can be as synthesized as lowpass filters.

However, it is difficult to extend this approach to higher frequencies due to the low capacitance required for the varactor diode. As frequency increases, the capacitance of the varactor must be smaller to operate in the same impedance range. The available phase shift range thus decreases for higher frequencies, using the conventional L-C approach. As will be discussed, the L-C approach also provides only a limited linear phase shift range.

In this chapter, tunable quasi-elliptic short-circuit terminated combline (STCL) filters are used as matched reactive loads (Figure 2.1). When the output port of the filter is shorted, the reflection phase is approximately two times the insertion phase, due to the double transit of energy through the filter. The usage of the two-pole STCL filters effectively doubles the linear reflection phase range of the tunable filter. Therefore, the achieved phase shift range is wider than that achieved with a single section L-C series resonant reactive load or with a similar matching network load and varactor diode. In this chapter, 360-degree linear phase shift was achieved at 5.2 GHz with a small tuning capacitance range (0.5 pF ~ 1.0 pF) and without cascaded couplers or sections. This design method can be applied at lower or higher frequencies. Design details and

measured data will be presented for the tunable short-circuit terminated combline filters used to implement the phase shifter.

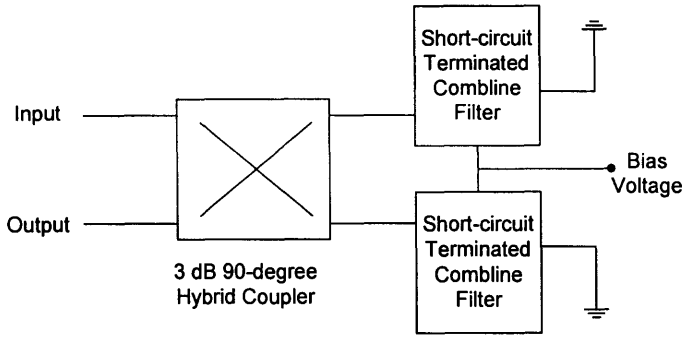

Figure 2.1 Phase shifter with the tunable short terminated combline filters as reactive loads.

2.2 Comparison of Tunable Short-Terminated Combline Filters With Conventional L-C Section Approach

Using L-C sections, the reflective circuit must be suitably designed to achieve the desired phase shift range, while maintaining as low an insertion loss as possible with voltage tuning. Figure 2.2 shows the response of several types of reactive loads. As the frequency increases, the varactor range must be smaller in order to get the same impedance range. In the case of higher frequency, it is difficult to get a wide phase shift range, because the required minimum capacitance of the varactor diode is too small. Thus, it is difficult to achieve the necessary capacitance variation. Instead of a single section L-C resonant load (Figure 2.2 (a)) or lowpass type (Figure 2.2 (b)), multiple higher order reactive loads can be used to get a wider phase shift range for higher frequency. In this case each varactor will require different capacitance ranges.

A microstrip combline topology can be used to produce a filter with an enhanced tuning range and compact size. The configuration of the proposed quasi-elliptic short

circuit terminated combline filter (STCL) is shown in Figure 2.2 (c). The STCL filters are connected to the 0-degree and 90-degree ports of the branch-line coupler, respectively. Other quadrature couplers, including Lange, lumped, and broadside-coupled lines can be used instead of the branch line coupler. The branch-line design is convenient for low-cost, planar implementation.

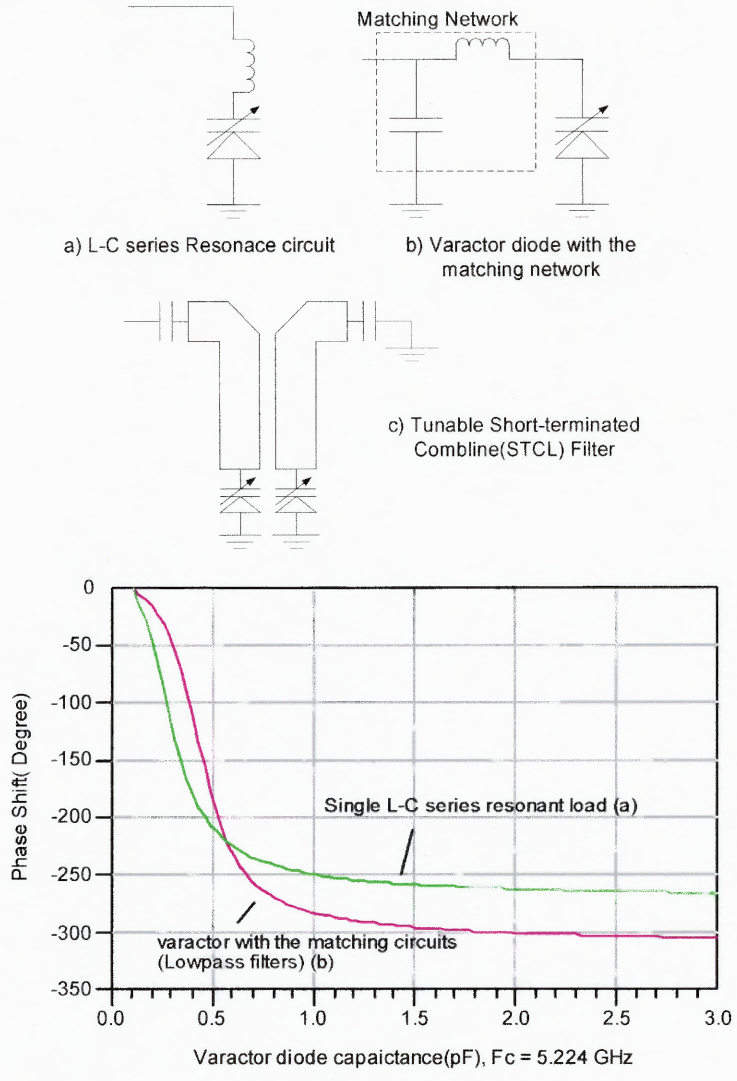

Figure 2.2 Simulated phase shift range of the reactive loads of a single L-C series resonant network; (a) and low a pass type matching network, (b) with the varactor diode capacitance (0.1 pF ~ 3 pF).

A two-pole STCL filter has a wider band linear transfer phase and reflection phase response over the pass band region, than does a two-element L-C section network, because the STCL filter order is effectively double that of L-C. When the output port of the filter is short terminated, the phase shift of reflected signal is almost twice the insertion phase (Figure 2.3). To actually see the response of the STCL filter, the filter is simulated with a terminating resistance of slightly greater than zero ohms. This allows for viewing the shape of the loss curve, which otherwise would be flatter. Figure 2.3 shows the simulated insertion and return loss for the coupled line pair, terminated with 0.2 ohms, with effective unloaded Q value of 250 for the filter.

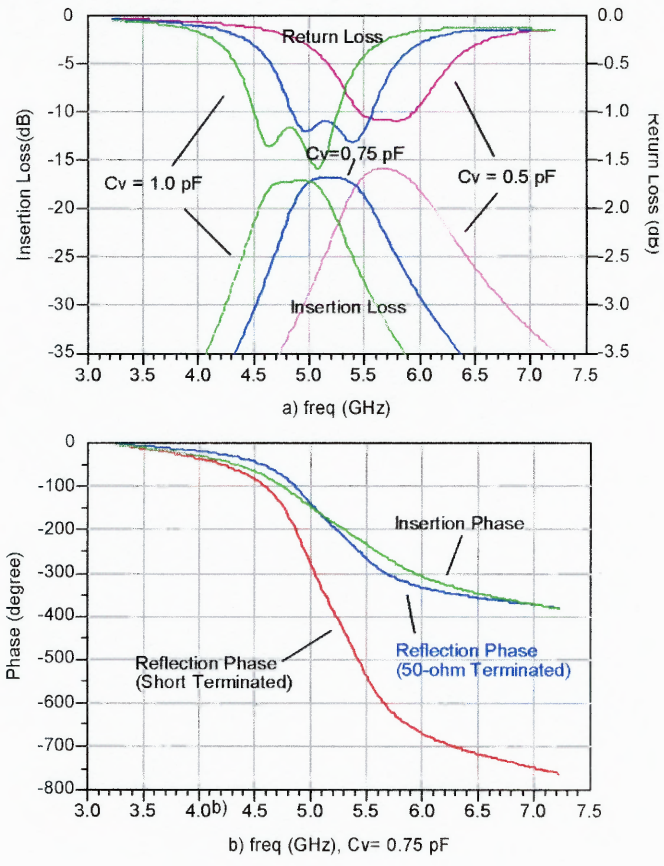

Figure 2.3 Simulated Insertion, return loss, and phase response of the tunable short-terminated filter.

The phase change for the phase shifter results from the changes in the reflection phase response of the filter. The filter is tunable, and so for any input frequency, displays a variable phase shift, due to motion along the phase response curve. Using this reflection phase, 360-degrees of linear phase shift can be achieved. For filter implementation a coupled parallel line pair with two identical varactor diodes was employed (Figure 2.2(c)). Figure 2.2(a) shows the insertion and return loss of the tunable short-terminated filter. Using 0.5 pF capacitance range, 1 GHz-tuning range was achieved, adequate for achieving 360-degrees of phase shift to any frequency in a 5.1 GHz to 5.3 GHz band.

The goal is to use the linear phase response region to get a 360-degree phase shift without the use of cascaded couplers. The advantage of an STCL filter is the 360-degree linear phase shift without cascading couplers. In this design, M/A COM GaAs Constant Gamma tuning varactor diodes (MA46H200-1056) are used, its capacitance at -2 volts is 1pF with capacitance ratio 3:1($C_{T\text{-}2}/C_{T\text{-}20}$) and Q=3000 at f=50 MHz, V=-4V.

$$\text{Output magnitude} \cong \tfrac{1}{2}(\Gamma_2 + \Gamma_1) \tag{2.1}$$

where Γ_2 and Γ_1 are the reflection coefficients of the two STCL filters ($|\Gamma|e^{j\phi}$)

Equation (2.1) shows a relationship between the output magnitude of the phase shifter and two reactive loads. If the two reactive loads are not identical, the insertion loss will increase. Figure 2.4 shows the output magnitude of the phase shifter vs. the difference of two reactive loads. When two reactive loads are perfectly matched, most of the energy is added up at the isolated port of the coupler. To evaluate the effects of unmatched diodes, Figure 2.4 shows how two different varactors affect the overall

insertion loss of the phase shifter. The diode mismatch causes some of the reflected energy to destructively interfere at the output port, resulting in amplitude ripple.

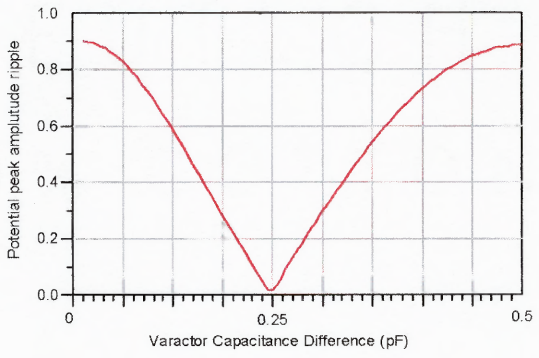

Figure 2.4 A potential peak amplitude ripple vs. difference of varactor diodes.(Fc=5.224 GHz).

2.3 Quasi-elliptic Filter Design

Various filters can be used as reactive loads to make the phase slope as steep as possible while preserving linearity, for a given filter bandwidth. In this chapter, the use of a quasi-elliptic network as shown in Figure 2.5 (a) and 2.6 (a) is suggested. This filter may be a two-pole open-circuited coupled transmission line pair, which differs from conventional combline filters. Unlike the conventional combline filter (Figure 2.5,6 (b)), which uses short-terminated parallel coupled lines (PCL), in the new approach the open-circuited end of the transmission line resonators are connected directly to input/output coupling networks. The negative coupling (due to the parasitic bridging capacitive coupling at this high E-field region of the open-circuited PCL) can be used to implement either a single or a pair of real-frequency transmission zeros near the filter passband [16]. Using only the parasitic capacitance naturally present, the single transmission zero resulting from the equivalent series tank circuit is too far from the passband region and does not add much phase slope. Enhancing negative coupling by moving the point of

connection such that input and output ports are negatively coupled, the two resulting transmission zeros can be moved toward the passband of the filter. In order to realize and move the transmission zeros, a bridge capacitor can be used (Figure 2.5,6 (c)). Instead of the bridging capacitor, a dielectric overlay (-'dielectric brick') can be used above the metal of the PCL (Figure 2.5,6 (e)). The technique is similar to that used with microstrip couplers to enhance directivity through equalization of the odd and even mode phase velocities. Alumina (Er= 9.8, tan δ=0.002, h=10mils) is used as a dielectric brick. Since the bridging brick is located inside the input/output-coupling transformer, only one transmission zero is introduced, because the equivalent is an L-C tank circuit in series acting as a coupling element. Thus, only the right transmission zero moves toward the passband region. The same effects can be observed in the conventional combline filter. Figure 2.5,6 (d) shows the quasi-elliptic filter of the conventional combline filter with the bridging capacitor. Adding an additional PCL section before the input/output coupling networks to the open-circuited quasi-elliptic filter (Figure.2.6 (a)) circuit, two transmission zeros can be moved toward passband together (Figure 2.5,6 (f)). The inductive coupling of an additional PCL with the input/output coupling capacitors makes two transmission zeros, one on each side of the passband [17].

The discussion in this section is based on the commercial E-M and circuit simulator (Sonnet, ADS). Table 2.1 shows the comparison of the phase slope of each filter. As can be seen, the open-circuited combline filter incorporating the "dielectric brick" has the steepest linear-region phase slope, in degrees/MHz. When these filters are used to provide reactive loads to the phase shifter, a larger phase shift combined with a wider linear region (linear in terms of the same number of degrees phase shift for any identical

bandwidth) can be achieved with the same bias voltage. To give more linear phase shift over a wider bandwidth, higher order filter can be used, or a transmission zero can be brought closed up to the passband (Figure 2.7).

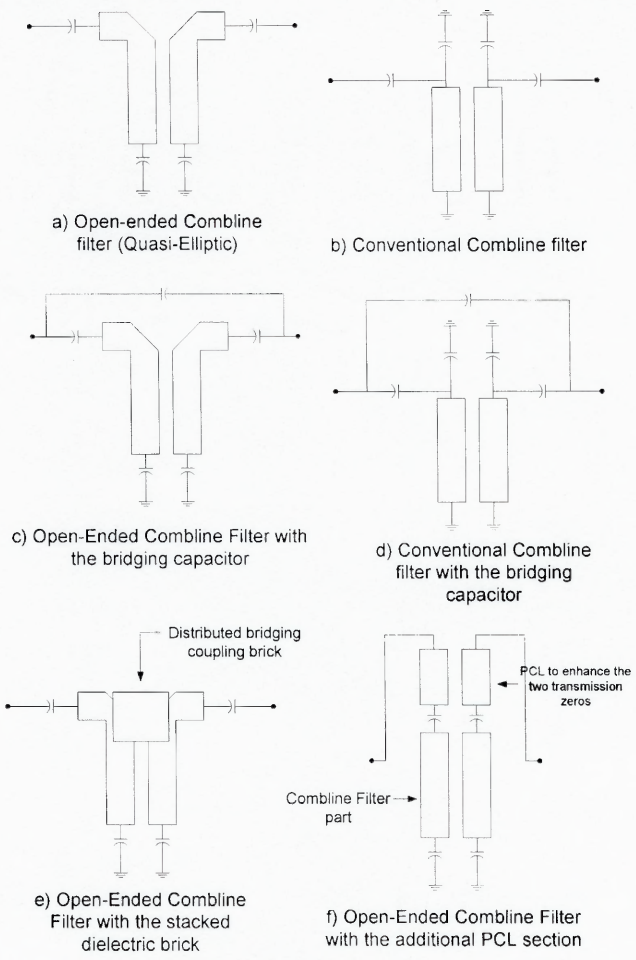

Figure 2.5 Various type of the two pole Combline filters.

Table 2.1 Phase Shift Slope Comparison as a Figure Merit of Degree/MHz ; Case (e) gives the steepest phase slope

Case (a)	0.177°/MHz
Case (b)	0.172°/MHz
Case (c)	0.189°/MHz
Case (d)	0.16°/MHz
Case (e)	0.193°/MHz
Case (f)	0.185°/MHz

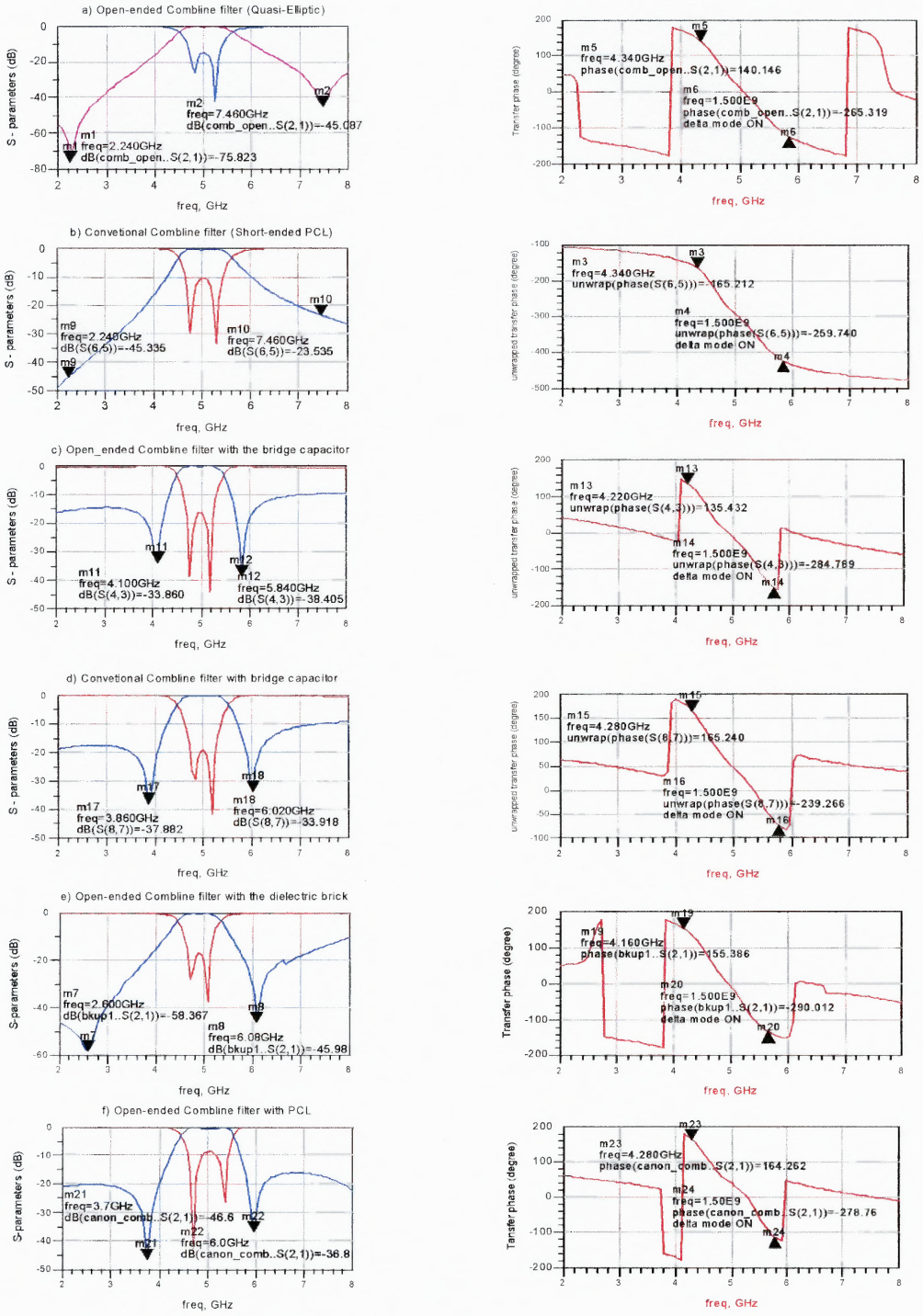

Figure 2.6 (a)~(f), Simulated S-parameters of the two-pole Combline bandpass filters, Fc= 5 GHz, BW= 600 MHz. $\varepsilon r = 2.94$, $\tan\delta = 0.001$ for the microstrip line, e) dielectric brick (Alumina: $\varepsilon r = 9.8$, $\tan\delta = 0.002$, thickness = 10 mils). The right marker in the phase response shows delta mode as a figure of merit of $\Delta\phi/\Delta f$.

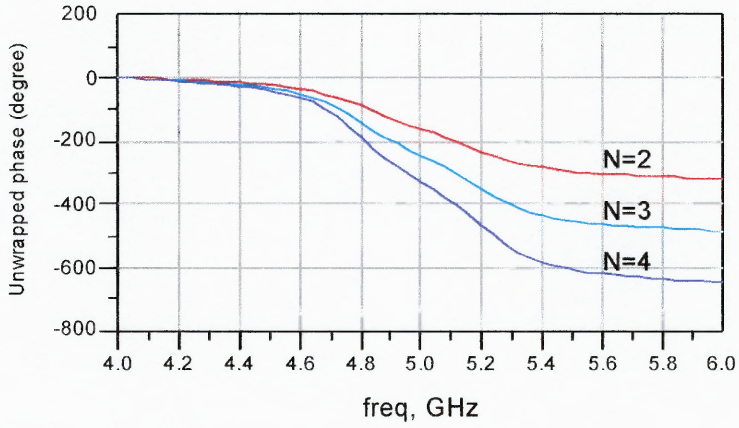

Figure 2.7 Comparison of the phase shift range in higher order bandpass filter (Fc= 5 GHz, BW= 600 MHz).

2.4 Results

For simulation of the phase shifter, HP Advanced Design System (ADS) is used [18]. The coupled line pair was synthesized using Filpro [19]. Figure 2.8 shows the phase shift angle vs. varactor diode capacitance. Using the tunable quasi-elliptic filters as reactive loads, over the 100MHz bandwidth the overall phase shift shows the same phase shift response shape: linear, as was required. Figure 2.9 shows the insertion loss and return loss of the phase shifter. The insertion loss is less than -1.5 dB and the return loss is less than -20 dB. Figure 2.10 shows the Smith chart of the reflection characteristics resulting from changing the varactor diode capacitance, at 5.224 GHz. The Smith chart illustrates that the very high reflection coefficient is maintained during varactor capacitance change, and thus low insertion loss is possible over the entire range of the phase shifter. The reactive load circle is very close to the purely constant reactive load circle. Figure 2.11 and Figure 2.12 show the preliminary measured data of the phase shifter at Fc = 5 GHz,

BW = 100 MHz. Figure 2.10 can be compared to Figure 2.4. Figure 2.8 shows the experimental amplitude ripple well within the limits illustrated in Figure 2.4.

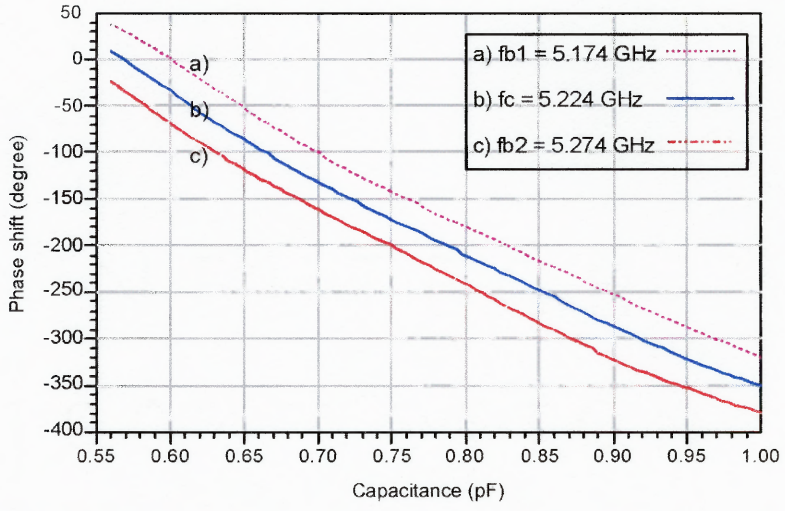

Figure 2.8 Simulated phase shift angles vs. varactor diode capacitance over 100MHz bandwidth, Fc = 5.224 GHz.

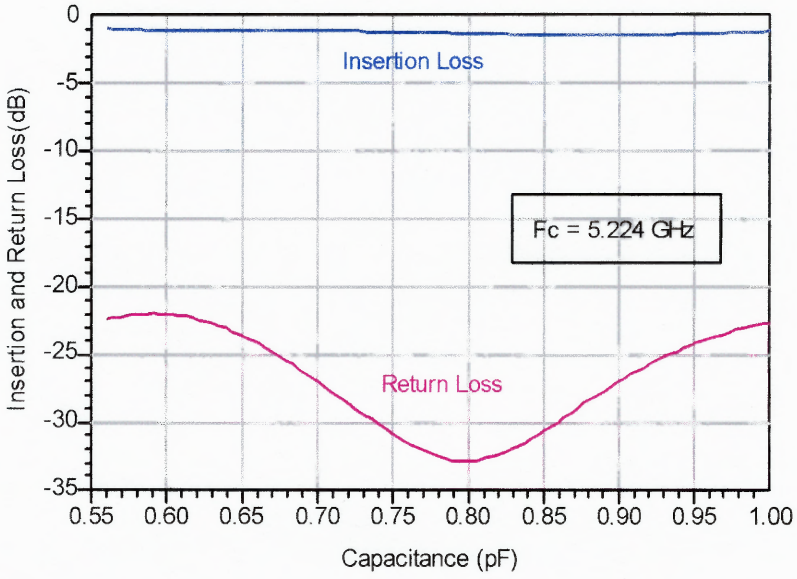

Figure 2.9 Simulated Insertion and Return loss of the phase shifter.

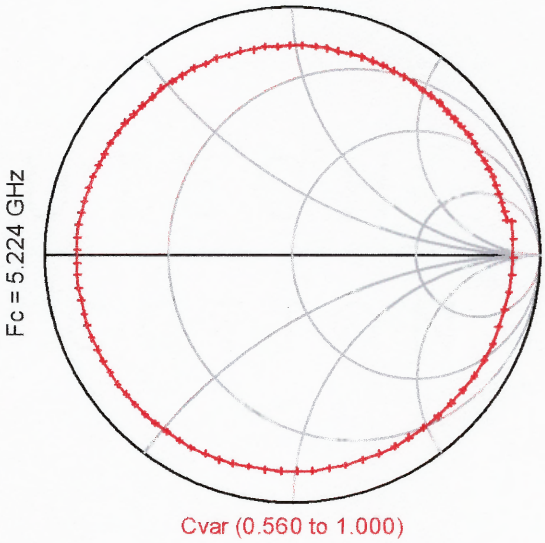

Figure 2.10 Simulated Smith Chart of the reflection characteristics resulting from changing the varactor diode capacitance (0.56 pF ~ 1.0 pF, Fc = 5.224 GHz).

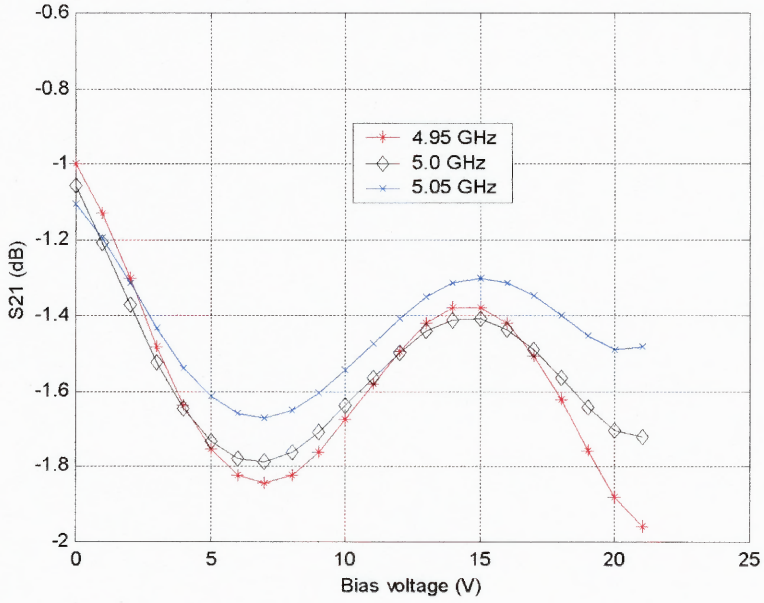

Figure 2.11 Measured amplitude response of the phase shifter.

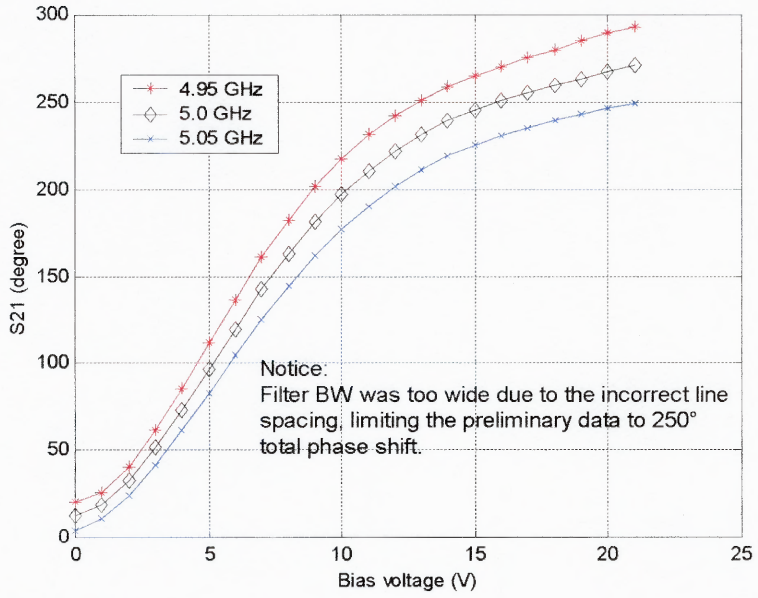

Figure 2.12 Measured phase response of the phase shifter.

2.5 Conclusions

The use of tunable quasi-elliptic short-terminated combline filters (STCL) as matched reactive loads on a 90-degree hybrid coupler has been shown to provide double the insertion phase of each filter. Because the use of circuit volume is more efficient with resonated coupled line sections than with single L-C sections (due to filter order doubling), the overall insertion loss is lower and phase shift range greater, than with the conventional L-C approaches. A two-pole quasi-elliptic combline pair has been shown to asymptotically approach 360-degree total phase shift, with a large linear range and an insertion loss of less than -1.5 dB over the full phase shift range. Extension to higher order combline or other coupled line networks should easily extend the phase shift range well beyond 360 degrees, and combline structures are practical at both higher and lower frequencies. To increase phase slope, a dielectric brick was used to enhance the bridging

capacitance of the quasi-elliptic filter. Other possible implementations of negative coupling will be explored in future work, to emphasize the achievement of large phase shift combined with linearity, over larger bandwidths. Incorporation of active devices other than conventional varactors is also possible, and might lead to efficient implementation of other system functions.

CHAPTER 3

CROSS-COUPLED RESONATOR FILTERS USING FREQUENCY INDEPENDENT AND DEPENDENT COUPLINGS

3.1. Introduction

Coupling matrices of the lowpass prototype filter have been widely used in direct–coupled resonator bandpass filter synthesis. Frequency invariable coupling matrices for a given topology can be obtained by using a lowpass prototype filter and ideal impedance inverters, combining with a sequence of similarity transformations and efficient optimization techniques [20]-[24]. In implementing the coupling matrix, the filter response is degraded to some extent and some kind of tuning and optimizations are required. Sometimes coupling coefficients from the coupling matrix may not be realizable. Under the frequency invariable coupling, *n-2* is the maximum number of finite transmission zeros (FTZs). This is theoretically verified for *n*-coupled resonator networks without source-load coupling [25]. In recent work [26], Amari *et al* prove when source-load coupling is involved, realizing *n* maximum finite transmission zeros from *n*-coupled resonators is possible.

However, the result is only valid for frequency invariable couplings. With a frequency-dependent inverter, a waveguide cavity filter that has more than *n* transmission zeros was reported [27]. In this chapter, the difference between the frequency-dependent coupling and independent coupling in filter response is discussed. An available method for source-load negative coupling in planar bandpass filter design is proposed. This result shows *n+1* finite transmission zeros out of *n* resonators. A two-pole combline filter with equivalent circuit is presented as an example.

3.2 Coupling Matrix Synthesis with Lowpass Prototype Filter

If the frequency band of interest is narrow, it can be assumed that coupling coefficients between the resonators is constant for the limited bandwidth. A network consisting of N-coupled loseless resonators with frequency independent couplings M_{ij} is shown in Figure 3.1. The loop equations for narrow bandwidths can be written as formula 3.1 [23]:

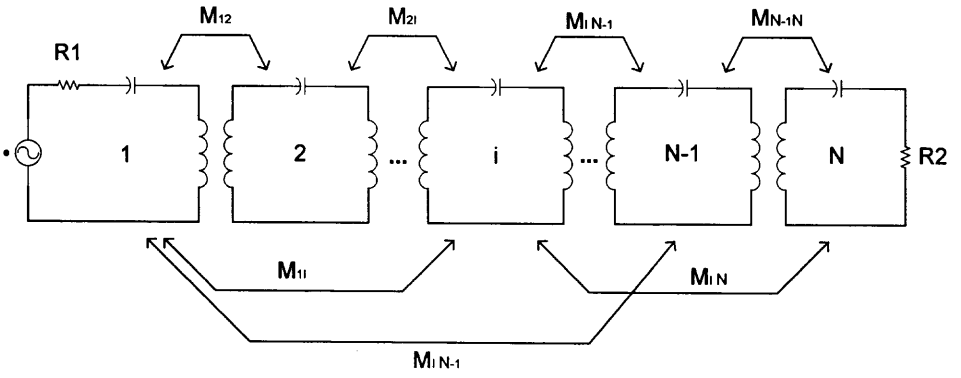

Figure 3.1 Model of general coupled resonator filter.

$$\begin{bmatrix} e_1 \\ 0 \\ 0 \\ \vdots \\ 0 \end{bmatrix} = \begin{bmatrix} s+R_1 & jM_{01} & 0 & 0 & \cdots & jM_{1n} \\ jM_{01} & s & jM_{12} & 0 & & \vdots \\ 0 & jM_{12} & s & jM_{23} & & \\ \vdots & & & \ddots & \ddots & \vdots \\ & & & & s & M_{n-1,n} \\ jM_{1n} & & & & \cdots & s+R_n \end{bmatrix} \begin{bmatrix} i_1 \\ i_2 \\ \vdots \\ \\ i_n \end{bmatrix} \tag{3.1}$$

or

$$[e] = [Z][I]$$

where

$$s = j(\omega - \frac{1}{\omega})$$
$$jM_{ij} \approx j\omega M_{ij} \approx j\omega_o M_{ij}\,.$$
$$\omega_o = 1 \text{ rad/sec}$$

In addition, the impedance matrix Z can be expressed in the form:

$$Z = (s*U + M_R) \tag{3.2}$$
$$U = \text{identity matrix}$$
$$M_R = R + j\,M.$$

As illustrated, the matrix R is a matrix which has nonzero values only if $R_{11} = R_1$ and $R_{NN} = R_2$. M is a symmetric square coupling matrix and has general entries of Mij for $i \neq j$, and 0 for i = j. s is normalized frequency.

[e] vector shows the excitation voltage $[e]^t = [1,0, 0,\ldots,0]$. The current vector [I] can be displayed with a new the matrix $[Z^{-1}]$.

$$[I] = [Z^{-1}][e] \tag{3.3}$$
$$[I] = [s*U + R + jM]^{-1}[e]$$

The scattering parameters is determined from the coupling matrix using the following formula [25].

$$S_{21} = 2\sqrt{R_1 R_2}\, I_N = 2\sqrt{R_1 R_2}\,[Z^{-1}]_{N1}$$
$$S_{11} = 1 - 2R_1 I_1 = 1 - 2R_1[Z^{-1}]_{11}. \tag{3.4}$$

In general, there are three ways to get a coupling matrix. The first way is the classical partial fraction expansion. Once a topology matrix is determined, a coupling matrix can be obtained by extracting each element value from the pre-determined transfer function. The resulting coupling matrix corresponds to the cascade of the extracted

sections [21]. The second way is to use repeated matrix similarity transformations (matrix rotations) to obtain desired couplings between resonators [22]. The third way is to use the optimization based on error functions to meet the specific poles and zeros locations of the transmission and reflection coefficients [28].

3.2.1 Coupling Matrix Synthesis Using Similarity Transformations

A similarity transformation on the N x N coupling matrix [Mo] is accomplished by pre- and post- multiplying coupling matrix [Mo] by N x N rotation matrix R and its transpose R^t as follows [22]:

$$[M_1] = [R]^t [Mo][R] \tag{3.5}$$

where [Mo] is the original coupling matrix, $[M_1]$ is the matrix after transformation, and the rotation matrix is defined in Figure3.2. Rii = Rjj = cos (θ_r), Rji = -Rij = sin (θ_r), (i, j $\neq$ 1 or N), and θ_r is the angle of rotation. Main diagonal elements are ones and all other entries except main diagonal elements are zeros.

$$[R]_r = \begin{bmatrix} 1 & 0 & 0 & 0 & 0 & 0 & 0 \\ 0 & 1 & 0 & 0 & 0 & 0 & 0 \\ 0 & 0 & \cos(\theta_r) & 0 & \sin(\theta_r) & 0 & 0 \\ 0 & 0 & 0 & 1 & 0 & 0 & 0 \\ 0 & 0 & -\sin(\theta_r) & 0 & \cos(\theta_r) & 0 & 0 \\ 0 & 0 & 0 & 0 & 0 & 1 & 0 \\ 0 & 0 & 0 & 0 & 0 & 0 & 1 \end{bmatrix}$$

Figure 3.1 Example of the rotation matrix R, θr is the rotation angle.

$$[Mr] = [Rr]^t \ [Mr_{-1}] \ [R_r], \qquad r = 1, 2, 3, \ldots, R \tag{3.6}$$

The principle of the rotational transformations is to be consecutively applied in the process and to cancel couplings until the coupling matrix of the cross-coupled array is transformed into the desired couplings. Since the eigenvalues of the admittance matrix are preserved even after transformations, transfer and reflection characteristics of the filter are the same. One drawback of this approach, however, is that the reduction process may not converge [28].

3.2.2 Numerical Example

A six-order linear phase filter is shown in Figure 3.3 as an example [39]. Matrix transformation will be performed to change the direction of input and output ports. The coupling matrix after a matrix rotation is displayed in Figure 3.3 (b). Ports are located in opposite directions.

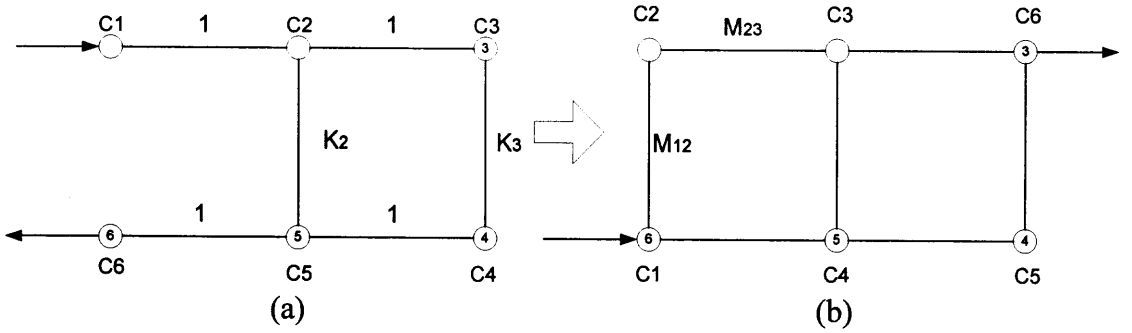

Figure 3.3 Cross-coupled lowpass prototype linear phase filter. Each circle shows the shunt capacitor.

The element values of the lowpass prototype of a generalized Chebyshev filter with the linear phase [39] are

$$C1 = 0.9822, \quad K1 = 0$$
$$C2 = 1.3912, \quad K2 = 0.1744$$
$$C3 = 1.9185, \quad K3 = 0.9265.$$

The even-mode coupling matrix in Figure 3.3 (a) is given by inspection as follows:

$$[K]=\begin{bmatrix} 0 & K_{12} & 0 \\ K_{12} & K_{22} & K_{23} \\ 0 & K_{23} & K_{33} \end{bmatrix} \tag{3.7}$$

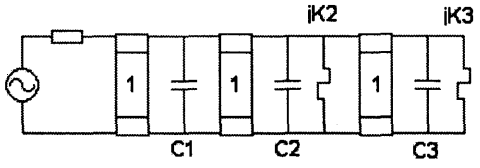

Figure 3.4 Even-mode equivalent circuit of the six-degree linear phase filter.

In order to eliminate the cross coupling between node 2 and node 5 in Figure 3.3 (a), transformed coupling matrix can be displayed as follows:

$$\begin{bmatrix} 0 & K_{12} & 0 \\ K_{12} & K_{22} & K_{23} \\ 0 & K_{23} & K_{33} \end{bmatrix} \rightarrow \begin{bmatrix} 0 & M_{12} & M_{13} \\ M_{12} & 0 & M_{23} \\ M_{13} & M_{23} & M_{33} \end{bmatrix} \tag{3.8}$$

The rotation matrix which can be applied is

$$[R]=\begin{bmatrix} 1 & 0 & 0 \\ 0 & \cos(\theta r) & \sin(\theta r) \\ 0 & -\sin(\theta r) & \cos(\theta r) \end{bmatrix}. \tag{3.9}$$

Transformed coupling matrix will have

$$[M] = [R]^t[K][R]. \tag{3.10}$$

After inserting a unity impedance inverter at the input, the even-mode circuit is shown in Figure 3.4. To make shunt capacitors at each node unity, row and column scaling factors are multiplied to the admittance matrix [Y].

$$
\begin{array}{cccc}
 & \frac{1}{\sqrt{C_1}} & \frac{1}{\sqrt{C_2}} & \frac{1}{\sqrt{C_3}} \\
 & \downarrow & \downarrow & \downarrow \\
[0 & j & 0 & 0] \\
[j & C_1 p & j & 0] \\
[0 & j & C_2 p + jK_2 & j] \\
[0 & 0 & j & C_3 p + jK]
\end{array}
$$

$$
[Y] = \frac{1}{\sqrt{C_1}} \rightarrow \quad \frac{1}{\sqrt{C_2}} \rightarrow \quad \frac{1}{\sqrt{C_3}} \rightarrow
$$

$$
= \begin{bmatrix}
0 & \frac{j}{(C_1)^{1/2}} & 0 & 0 \\
\frac{j}{(C_1)^{1/2}} & p & \frac{j}{(C_1C_2)^{1/2}} & 0 \\
0 & \frac{j}{(C_1C_2)^{1/2}} & p + \frac{jK_2}{C_2} & \frac{j}{(C_1C_2)^{1/2}} \\
0 & 0 & \frac{j}{(C_1C_2)^{1/2}} & p + \frac{jK_3}{C_3}
\end{bmatrix}
$$

$$
= \begin{bmatrix}
0 & j1.009 & 0 & 0 \\
j1.009 & p & j0.85547 & 0 \\
0 & j0.85547 & p + j0.12536 & j0.6121 \\
0 & 0 & j0.6121 & p + j0.4829
\end{bmatrix} \tag{3.11}
$$

Coupling matrix element values before the transformations are

$$K_{12} = 0.85547$$

$$K_{22} = 0.12536$$

$$K_{23} = 0.6121$$

$$K_{33} = 0.4829.$$

From [39]

$$t_1 = \tan(\theta_1) = \frac{K_{23} + (K_{23}^{\ 2} - K_{22}K_{33})^{1/2}}{K_{33}} = 0.1069 \text{ or } 2.4282$$

After taking small value t_1, coupling coefficients are

$$M_{12} = C_1 K_{12} = 8.8506$$

$$M_{13} = S_1 K_{12} = 0.0910$$

$$M_{23} = K_{23} - K_{33} t_1 = 0.5605$$

$$M_{33} = K_{22} + K_{33} = 0.6083$$

From the (3.8), the resulting even-mode coupling matrix is

$$\begin{bmatrix} 0 & 0.85547 & 0 \\ 0.85547 & 0.12536 & 0.6121 \\ 0 & 0.6121 & 0.4829 \end{bmatrix} \rightarrow \begin{bmatrix} 0 & 8.8506 & 0.0910 \\ 0.8506 & 0 & 0.5605 \\ 0.0910 & 0.5605 & 0.6083 \end{bmatrix}.$$

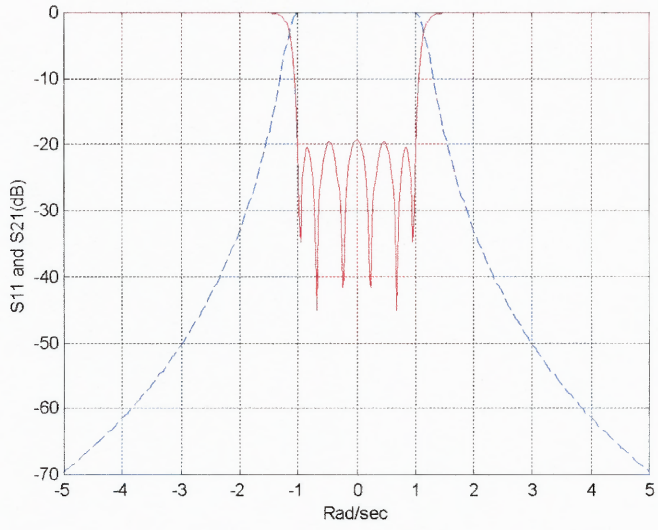

Figure 3.5 Simulated response of the transformed bandpass filter.

3.3 Coupling Matrix Synthesis Using a Numerical Optimization

A frequency-independent coupling matrix for the cross-coupled resonator filters can be determined from the numerical optimization method [28],[29]. A general cross-coupled resonator bandpass filter is shown in Figure 3.1. From the loop currents, a matrix equation can be displayed with the coupling matrix as follows:

$$[\omega U - jR + M][I] = [A][I] = -j[e], j^2 = -1.$$

Here, M is a symmetric square coupling matrix, R is a matrix which has nonzero values only if $R_{11} = R_1$ and $R_{NN} = R_2$, and [U] is the identity matrix. [e] vector shows the excitation voltage $[e]^t = [1,0, 0,\ldots,0]$.

The current vector [I] can be displayed with a matirx [A].

$$[I] = -j[A^{-1}][e]$$

The scattering parameters are determined from the coupling matrix.

$$S_{21} = 2\sqrt{R_1 R_2} I_N = -2j\sqrt{R_1 R_2}[A^{-1}]_{N1}$$
$$S_{11} = 1 - 2R_1 I_1 = 1 + 2jR_1[A^{-1}]_{11}.$$

The optimization procedure begins with an initial guess for the coupling matrix. A simple initial guess for the coupling matrix is the topology matrix. The error function for the optimization is based on the values of the gradient of S_{11} and S_{21} [28].

$$\text{Errf} = \sum_{i=1}^{N} [S_{11}(A_i)]^2 + \sum_{j=1}^{m} [S_{21}(B_j)]^2 + [\varepsilon - \hat{\varepsilon}]^2 \qquad (3.12)$$

where the functions S_{11}, S_{21}, and ε^ are evaluated from the current trial matrix M, and ε is the desired scale factor related to the pass band ripple in the insertion loss filter function. An unconstrained search optimization algorithm can be used to minimize error function. A numerical optimization result is displayed in Figure 3.6 as an example [28].

$$M = \begin{bmatrix} 0 & 1 & 0 & 0 & 0 & 1 \\ 1 & 0 & 1 & 0 & 1 & 0 \\ 0 & 1 & 0 & 1 & 0 & 0 \\ 0 & 0 & 1 & 0 & 1 & 0 \\ 0 & 1 & 0 & 1 & 0 & 1 \\ 1 & 0 & 0 & 0 & 1 & 0 \end{bmatrix} \Rightarrow \begin{bmatrix} 0 & 0.8298 & 0 & 0 & 0 & 0.0194 \\ 0.8298 & 0 & 0.5789 & 0 & -0.1658 & 0 \\ 0 & 0.5789 & 0 & 0.7060 & 0 & 0 \\ 0 & 0 & 0.7060 & 0 & 0.5789 & 0 \\ 0 & -0.1658 & 0 & 0.5789 & 0 & 0.8298 \\ 0.0194 & 0 & 0 & 0 & 0.8298 & 0 \end{bmatrix}$$

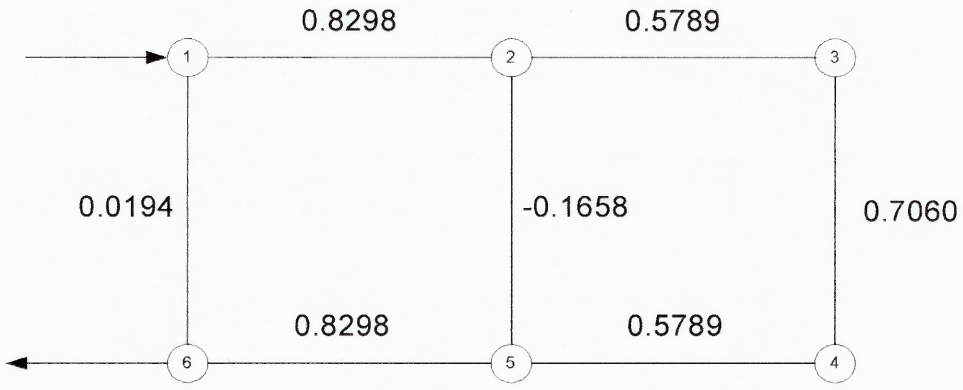

Figure 3.6 Coupling matrix and completed circuit values.

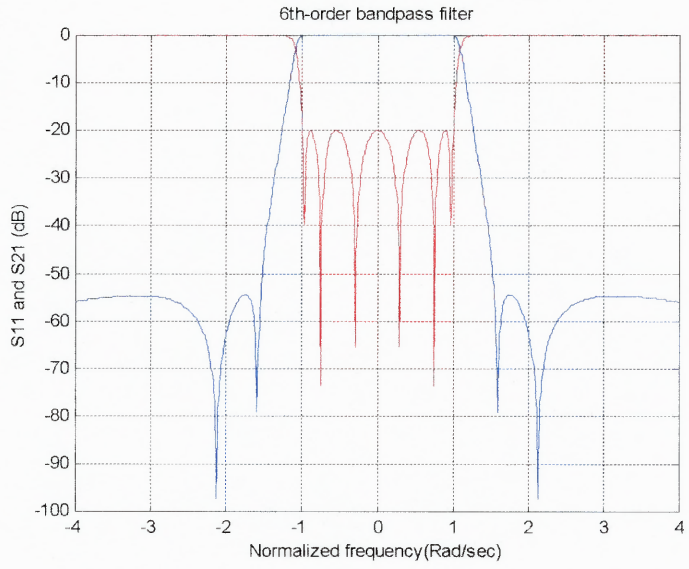

Figure 3.7 Simulated filter response of the optimized coupling matrix.

3.4 Cross-coupled Filter Design and Experimental Results

The approach using the frequency-independent coupling matrix is quite accurate for the narrow-band filter synthesis. However, this method does not show filter response in the rejection band in an accurate manner [30]. A two-pole bandpass filter which has a negative cross coupling from source to load is shown in Figure 3.8. The cross-coupled inverter has the negative impedance (–K) to make a negative source-load coupling with respect to the main coupling. An achievable practical circuit after Pi-transformation of ideal inverters is shown in Figure 3.8 (b). When positive source-load coupling is employed, two finite transmission zeros (FTZs) can be obtained, i.e., n maximum FTZs out of n resonators. The negative source-load coupling gives $n+1$ FTZs (Figure 3.9), since the negative coupling interacts with the main coupling elements. To obtain extra FTZs, inductors are used as impedance transformers. The negative cross coupling (capacitive) and main coupling (inductive) make three FTZs on the imaginary axis and show asymmetrical insertion loss in the rejection band.

To get closer lower-side two FTZs, the original circuit of Figure 3.8 (b) is tuned to the response of Figure 3.10. Since coupling coefficients are actually frequency variable, evaluation over the wide frequency range shows that ideal frequency invariable inverters do not correctly predict extra FTZs in the rejection band. As seen in Figure 3.9, near the center frequency of the filter, both cases are well matched. However, far away from the center frequency, the filter response is quite different. Thus, the truly frequency variable couplings must be taken into account to correctly predict the filter stopband performance. This phenomenon can be utilized to improve filter performance, by moving the extra TZ closer to the passband.

To apply this approach to the practical circuit and control the TZ's location in the stopband, a combline filter is used (Figure 3.11). The main coupling between parallel-coupled lines of combline filter is inductive coupling. This inductive coupling and inductors, as impedance transformers, can be used to make the extra TZ with the capacitive source-load cross coupling. An equivalent circuit of the cross-coupled combline filter is shown in Figure 3.12.

However, the required capacitive coupling in the circuit of Figure 3.10 (see Table. 1) is so weak that it is not easy to realize as a conventional capacitor. The use of a dielectric block metalized on the top surface to realize an inhomogeneous transmission line is proposed, to achieve the capacitive source-load coupling in combline filter (Figure 3.11).

The advantage of this approach is that the required cross coupling value is realized by changing the substrate thickness, dielectric constant, top metal size or length of the dielectric block. Connection wire size effects (lead inductance) can be avoided. An approximate calculation for the overlapping conductor size of the cross coupled-transmission line block is determined by parallel plate capacitance formula (Figure 3.12). Values of the cross coupling block and other combline filter parameters are displayed in Table 1. An EM-Circuit Co-simulated filter response, using the inhomogeneous transmission line dielectric block, is illustrated in Figure 3.13.

Table 3.1 Values of Components for Circuits in Figure 3.8, 3.10, and 3.12 ($R_s=R_L=50$ Ohms); Inverter are converted at Fc = 5 GHz

Ideal inverters	Real Circuit (Figure 1)	Tuned Circuit (Fig. 3)	Cross-coupled Combline Bandpass filter (Figure 4)
$K_{S1} = K_{2L} =$ 237.21	$L_{S1} = L_{2L} = 7.381$ nH	$L_{S1} = L_{2L} =$ 1.7799 nH	$L_1=L_2 = 8.4$ nH, Q=1200 @ 5GHz
$K_{12} =$ 1125.3	$L_{12} = 89.56$ nH	$L_{12} = 3.582$ nH	Short Circuit stub = 280 mils, Line gap = 90 mils
$K_{SL}= -2400$	$C_{SL} = 0.013$ pF	$C_{SL} = 0.006$ pF	Cross sectional size for cross coupling capacitance = 50 x 50 mils, $\varepsilon_r =2.38$, h = 60 mils
Lr = 1.013 nH, Cr =1 pF(Resonators)	Lr = 1.2059 nH, Cr =1 pF(Resonators)	Lr = 0.107825 nH, Cr =10 pF(Resonators)	Cr = 0.35 pF, Q =1200 @5 GHz (Resonators)
	$L_{sh} = 76.394$ nH due to the Pi-conversion of negative – K inverter.		

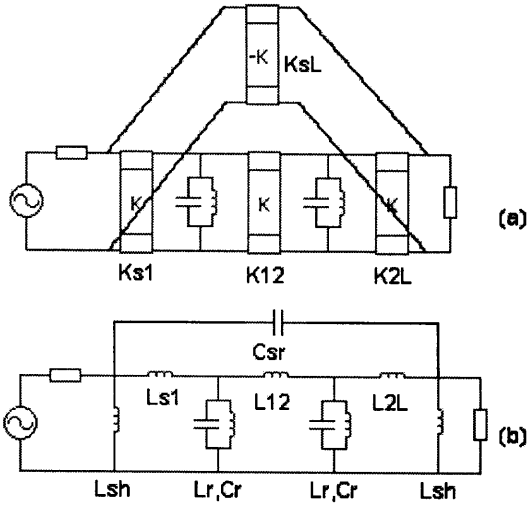

Figure 3.8 Source-load negative coupling two-pole filter; (a) Frequency-independent ideal inverter negative source-load coupling (-K), (b) Frequency-dependent with a negative source-load coupling after Pi-inverter transformations.

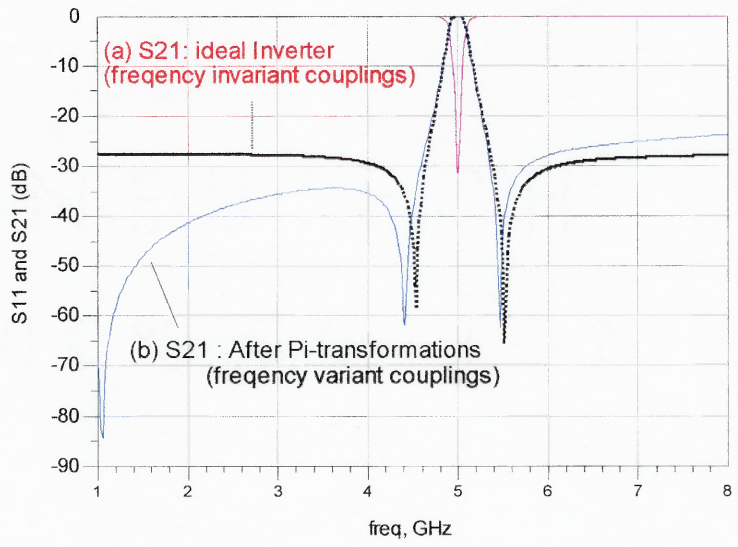

Figure 3.9 Two pole filter response comparison with a negative source-load coupling between frequency invariable and variable couplings.

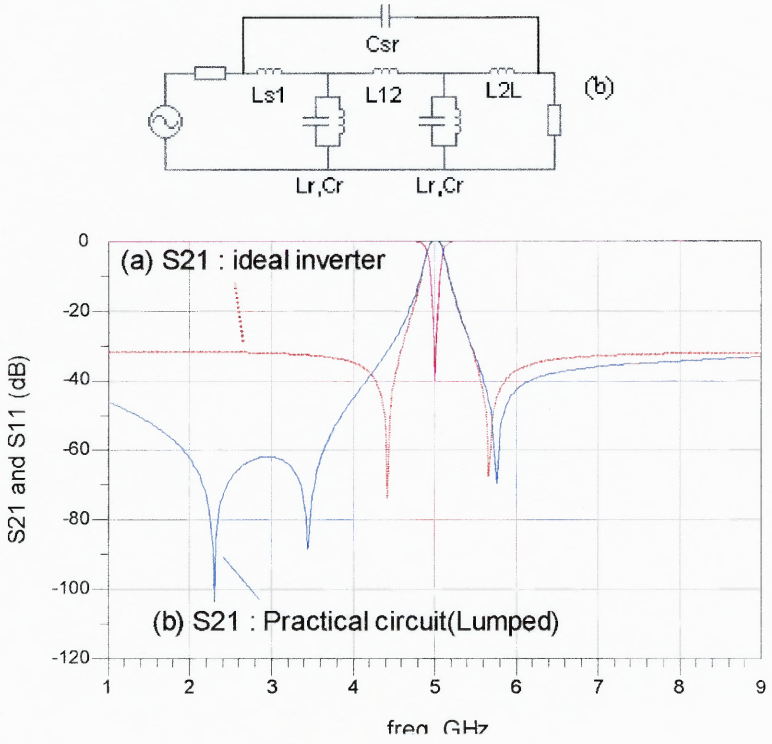

Figure 3.10 Insertion and return loss with three FTZs after tuning and an equivalent circuit

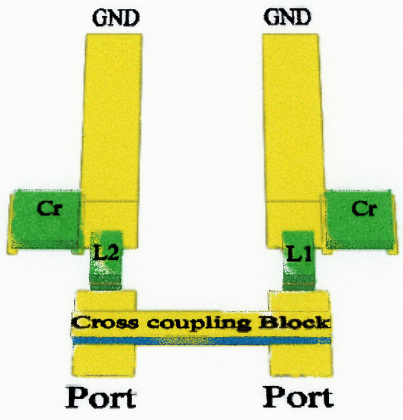

Figure 3.11 Two-pole combline filter with the top metalized dielectric block for source-load coupling.

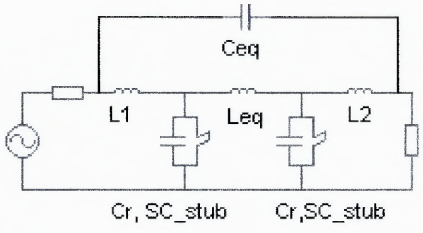

where $Ceq = \frac{\varepsilon r * A}{t}$,

Leq = Net coupling between parallel-coupled lines

A : cross-sectional top and bottom metal size

t : dielectric substrate thickness

Figure 3.12 An equivalent circuit for Figure 3.11.

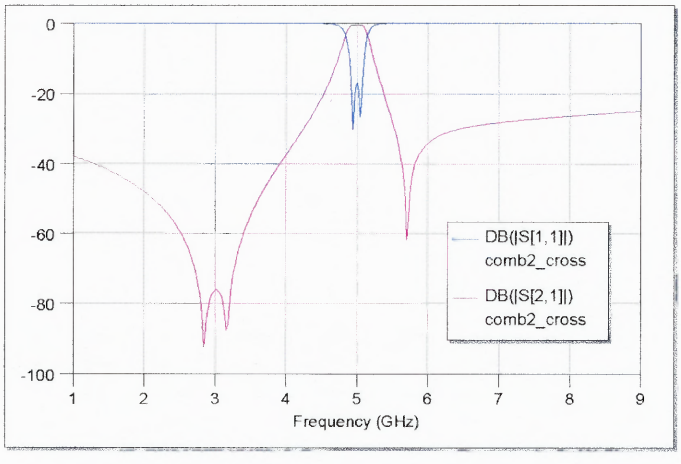

Figure 3.13 EM-Circuit Co-simulated filter response of the combline filter using a negative source-load coupling block.

3.5 Cascaded Effect of the Same Two-pole Cross-Coupled Network

The purpose of this section is to see the cascading effect of the same two-pole cross-coupled bandpass filter. For the reference filter of the comparison, a four-pole bandpass filter with a negative source-load coupling is shown in Figure 3.14. Two FTZs are obtained due to the source-load cross-coupling network. It does not show extra TZs in this simulation.

Figure 3.15 shows the two-pole bandpass filter which will be cascaded to make a four-pole filter. The filter response is shown in Figure 3.14 after directly connected without any extra coupling between the two building blocks (two-pole cross-coupled BPF). The passband response is acceptable, however, the return loss except the pasband region shows spurious transmission poles in the stopband area.

When inverter is involved between the same two-pole cross-coupled networks, the overall insertion loss is improved, showing the same number of FTZs as the two-pole bandpass filter (Figure 3.17(a)). Thus, in order to be used as a cascaded filter, either extra capacitive or inductive coupling is necessary. The insertion loss of the cascaded filter with an inverter is much better than four-pole BPF with a source-load negative coupling (Figure 3.17(b)). A drawback of the source load-coupling filter is the poor stopband response of the insertion loss. A cascaded two-pole cross-coupled network can improve the weakness of the rejection response of the source-load coupling filter and shows possibility as cascaded filter elements which has the FTZs, such as Cascaded Triplet (CT) or Cascaded Quadruplet (CQ) filters (Figure 3.17(c)).

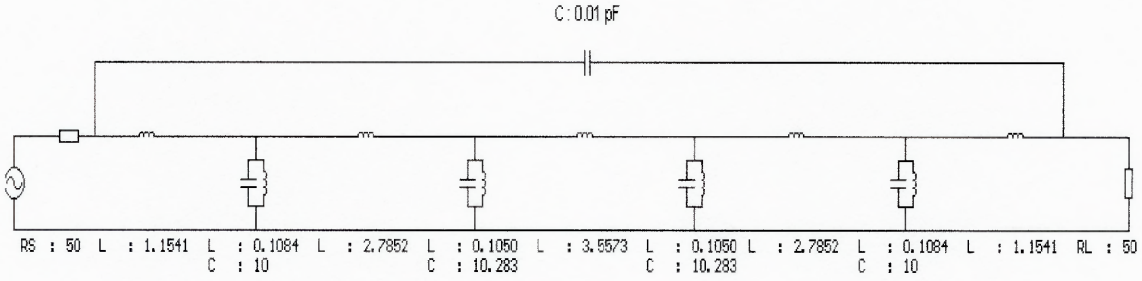

(a)

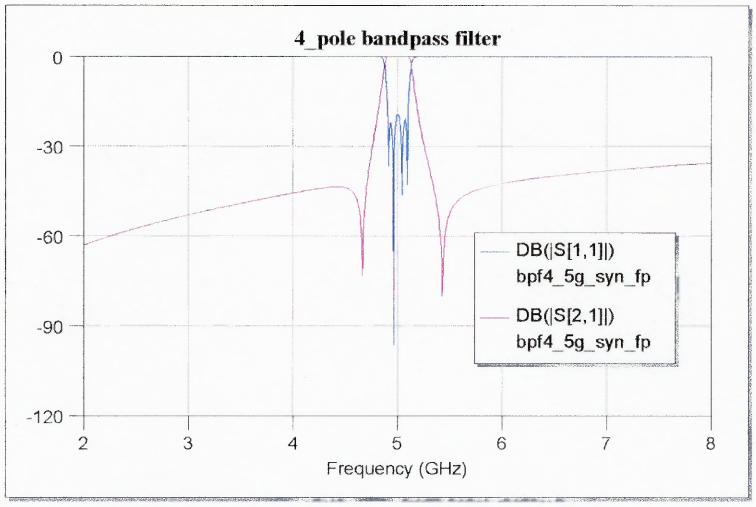

(b)

Figure 3.14 A four-pole bandpass filter with a negative source load coupling; (a) Schematic (b) Insertion and return loss.

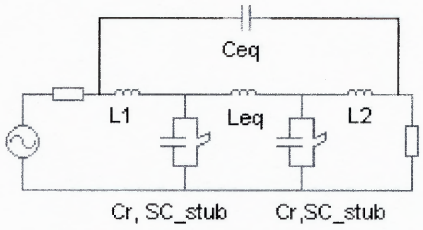

(a)

Figure 3.15 two-pole combline filter with a source-load negative coupling. (a) Schematic.

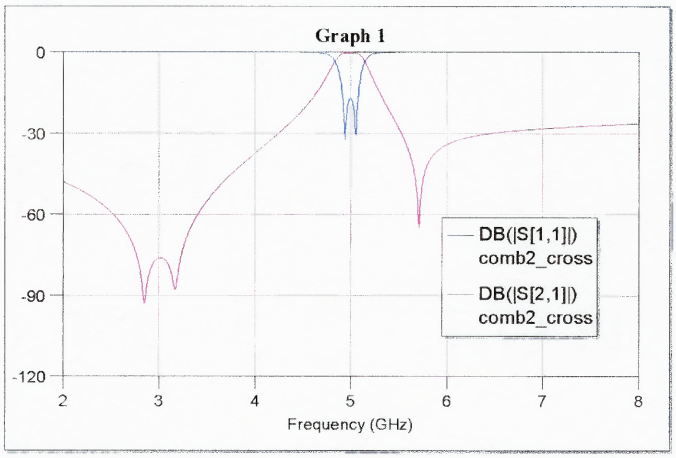

(b)

Figure 3.15 two-pole combline filter with a source-load negative coupling; (b) filter response (continued).

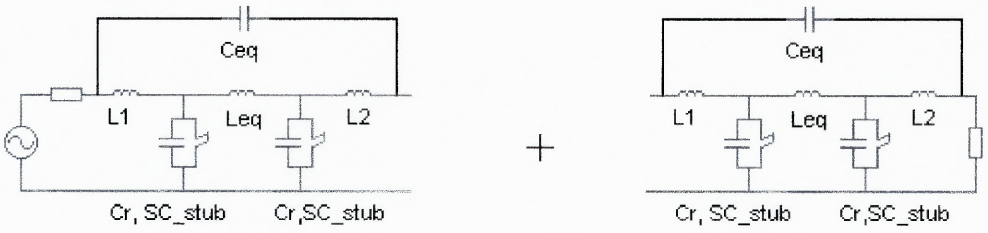

(a)

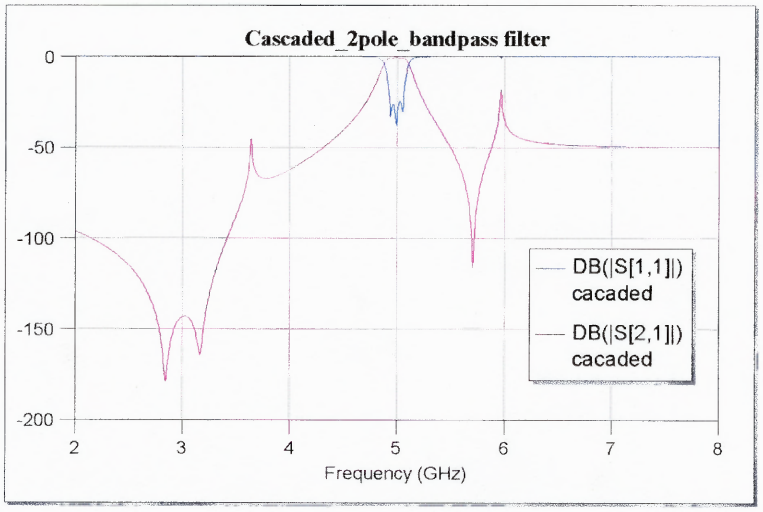

(b)

Figure 3.16 Directly cascaded filter with two-pole cross-coupled Bandpass filter; (a) Schematic, (b) filter response.

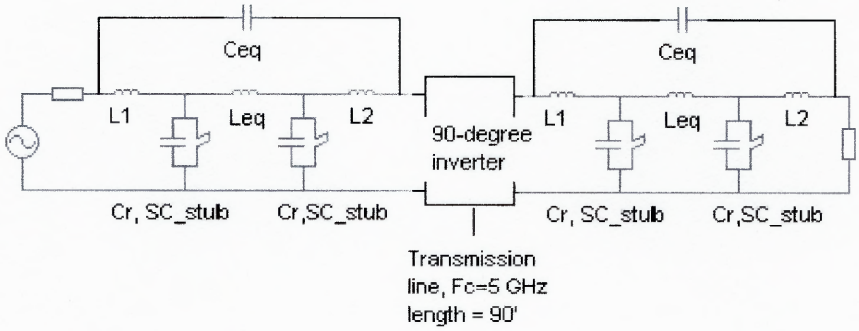

(a)

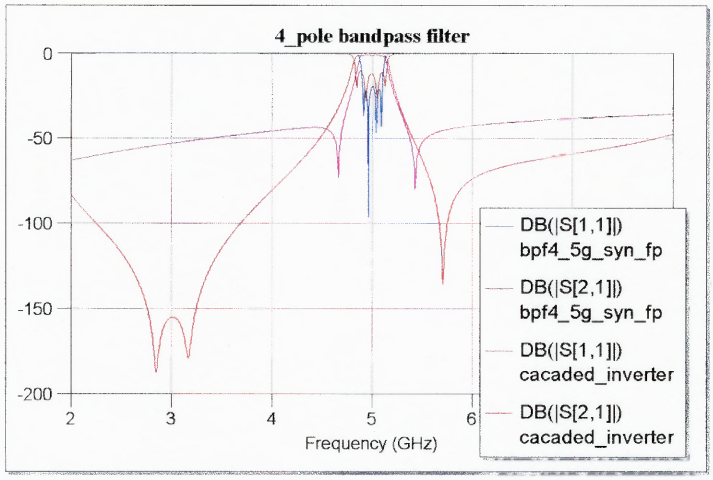

(b)

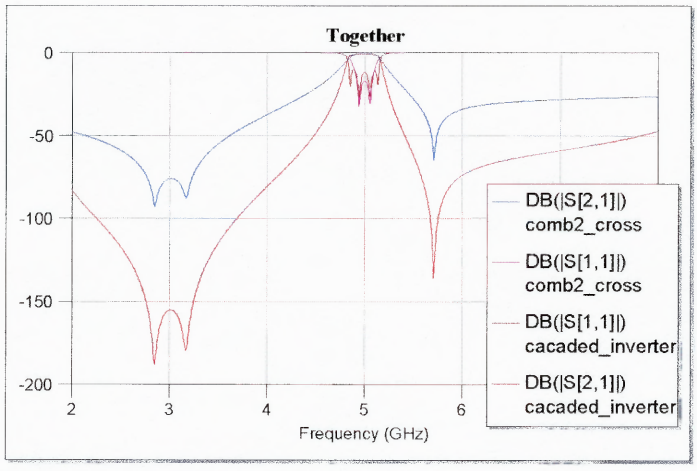

(c)

Figure 3.17 Cascaded four-pole bandpass filter with 90 degree inverter between the same two-pole BPF; (a) schematic, (b) insertion and return loss (pink curve : 4-pole BPF with a source load coupling, red curve : cascaded two-pole BPF with a inverter), (c) insertion loss and return loss.(blue curve : two-pole cross coupled BPF, red curve – cascaded two-pole BPF with a inverter).

3.6. Conclusions

This chapter examined the difference between the filter response computed assuming frequency invariable couplings from the real response based on real frequency variable couplings. It is proposed that the "real" couplings should be utilized to predict and achieve extra TZs by intentionally emphasizing the effect of the frequency variation. An efficient top metalized dielectric block overlay to be used in the planar bandpass filter design is presented for the source-load cross coupling.

CHAPTER 4

TUNABLE FILTERS

4.1 Introduction

Almost all filters can be tuned by varying the electrical lengths of resonators, or by introducing some form of variable capacitive or inductive loading in the resonators. Resonator Q values, tuning speed, tuning method, and temperature compensation etc. can be considered as design factors for tunable microwave filters.

Generally, tunable filters have narrow bandwidth. A requirement is thus imposed on the minimum Q necessary for each resonator of the resultant filter. Such filters rely on the electromagnetic coupling between resonators through the impedance inverting circuit element [41]. Since the couplings are unavoidably frequency dependent, impedance inverters designed assuming frequency independence only conform to design assumptions over a limited narrow bandwidth. There are many possible means for adjusting the bandwidth of a tunable filter. However, the bandwidth of conventional designs is typically proportional to the center frequency.

$$\text{Bandwidth}_{F02} = (F_{02}/F_{01}) * \text{Bandwidth}_{F01} \tag{4.1}$$

In some cases, it is desirable to maintain constant absolute bandwidth as center frequency is varied, or even to modify the rejection characteristics as the center frequency is varied by tuning finite frequency transmission zeros.

Mechanically tunable microwave filters were widely used in old communication systems. Modern communication systems require fast tuning speeds. Hence, the electrically tunable filter would be a more desirable approach.

In this chapter, conventional approaches for the tunable filters will be presented with the planar types of bandpass filters. Computer analyses of such filters are introduced for the frequency-independent and frequency-dependent coupling cases. Finally, a tunable transmission zero filter using the cascaded cross-coupled network will be presented.

4.2 Conventional Tunable Filter

In general, bandpass characteristics can be varied within a desired frequency range. Available techniques take account of varactor diodes [32], ferrite-slab loaded evanescent-mode waveguide [39], ferroelectric substrate [35], and ferromagnetic material [36].

When varactor diodes are involved in the resonators and coupling circuit network, the center frequency and bandwidth of the bandpass filter can be tuned. The advantages of such an approach are small size and fast tuning speed compared to the Yttrium-Iron-Garnet (YIG) tuned filter. In recent work [33], a millimeter-wave planar tunable filter was fabricated on the thin membrane using the Micro-Eletro-Mechanical Systems (MEMS) technique. Despite such an advantage, the application of varactor-tuned filters may be restricted by low power handling and low Q value of varactor diodes, which implies some difficulties in making narrowband filters. As a solution to the low Q value problem, negative resistance methods, which use MMIC combined with varactor diodes, can be used [15].

In this section, conventional tunable filter design methods are applied to the planar filter structure. A three-pole tunable bandpass filter circuit is shown in Figure 4.1 as an example. Each resonator is connected through the frequency-independent impedance

inverters. As seen in this example, only inductors of the each resonator are considered as a tuning factor. According to the Table 4.1, every component value is kept constant including coupling coefficients over the entire tuning range, except the inductance of each resonator. Component values are obtained using the Filpro filter synthesis tool [19]. Figure 4.2 shows the consistent bandpass filter response over 2 GHz tuning range with the same 200 MHz bandwidth. Thus, the required real coupling-circuit values for each tuning range can be calculated from the Pi-transformations of the ideal inverters. The obtained values can be used for the bandwidth variation compensation along the tuning range. This would serve as an advantage of the frequency-independent coupling approach for the tunable filter design.

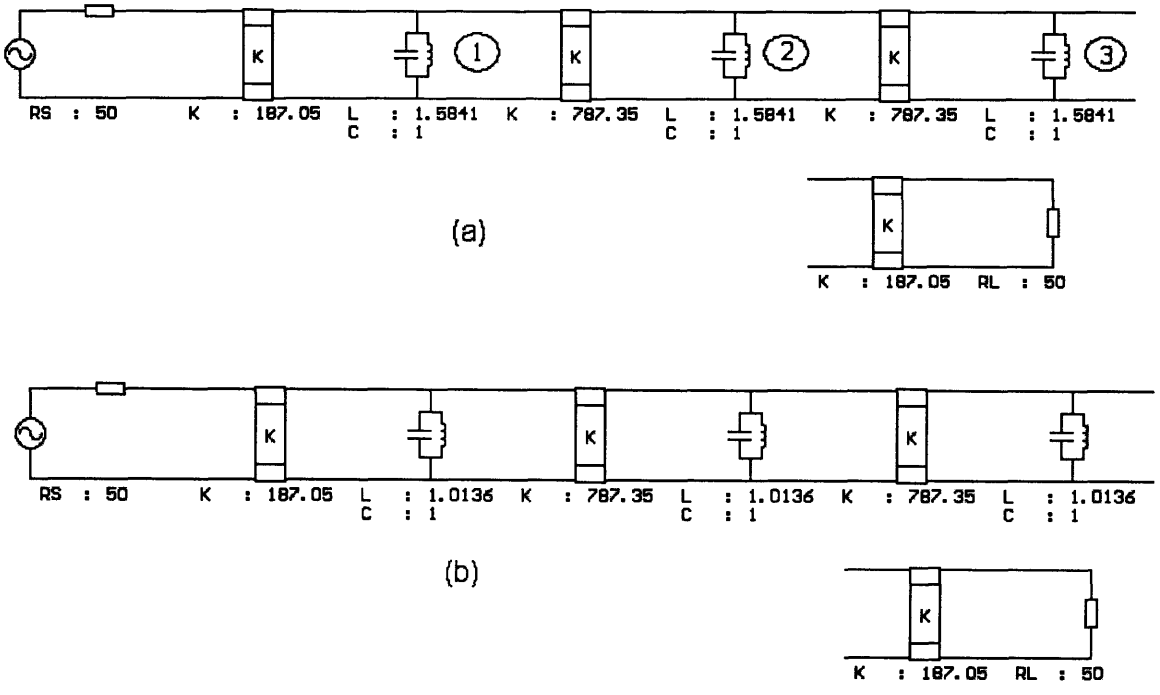

Figure 4.1 Three-pole tunable bandpass filters with bandwidth 200MHz; Inductors of resonators are tuning components; (a) Fc = 4GHz, (b) Fc = 5GHz

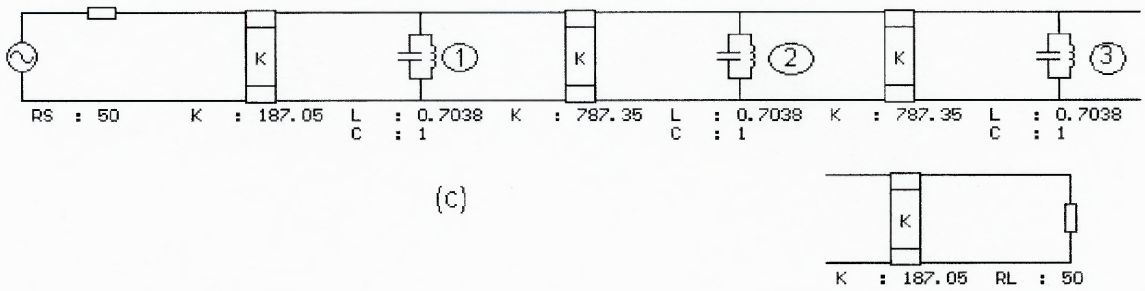

Figure 4.1 Three-pole tunable bandpass filters with bandwidth 200MHz; Inductors of resonators are tuning components; (c) Fc = 6 GHz (continued).

Table 4.1 Component Values of the Three-pole Tunable Filter as shown in Figure 4.1

	Case(a): fc = 4 GHz	Case(a): fc = 5 GHz	Case(a): fc = 6 GHz
	K_{s1} = 187.05	K_{s1} = 187.05	K_{s1} = 187.05
Resonator 1	L_1=1.5841, C_1 =1	L_1=1.0136, C_1 =1	L_1= 0.7038, C_1 =1
	K_{12} = 787.25	K_{12} = 787.25	K_{12} = 787.25
Resonator 2	L_2=1.5841, C_2=1	L_2=1.0136, C_2=1	L_2=0.7038, C_2=1
	K_{23} = 787.35	K_{23} = 787.35	K_{23} = 787.35
Resonator 3	L_3=1.5841, C_3=1	L_3=1.0136, C_3=1	L_3=0.7038, C_3=1
	K_{3L} = 187.05	K_{3L} = 187.05	K_{3L} = 187.05

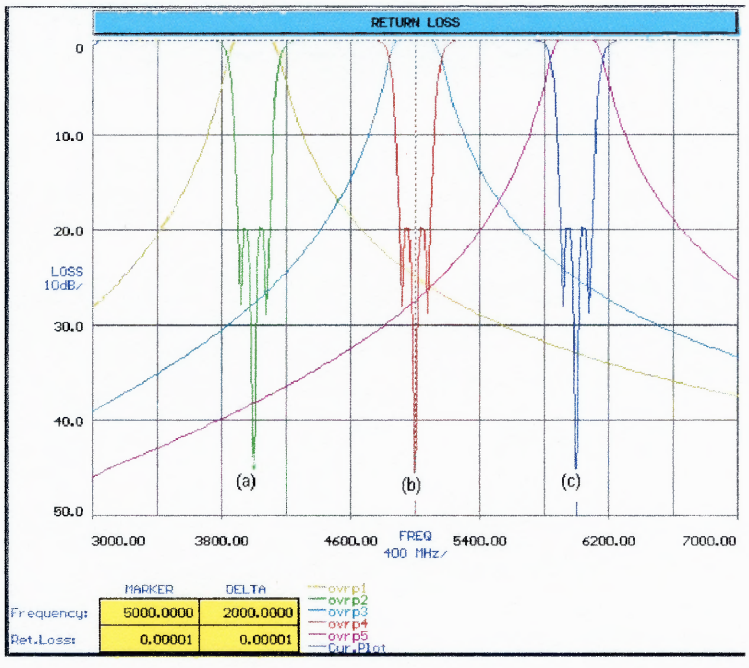

Figure 4.2 Filter response of the three-pole tunable filters (BW; 200 MHz, Tuning range; 4 GHz - 6 Hz).

The dielectric constant of the ferroelectric substrate varies in accordance with the DC biasing electric field. When a tunable material such as ferroelectric substrate is used, the center frequency of the filter can be tuned without extra varactor diodes [35]. A four-pole interdigital bandpass filter, which uses a ferroelectric substrate, is illustrated in Figure 4.3. EM-simulator results are displayed in Figure 4.4. This simulation is performed with the dielectric constant range from 1.94 to 3.94. This range actually does not represent the real dielectric constant variation of a practical ferroelectric material. In this simulation, the variation is used to show the tuning effects which a tunable dielectric constant substrate would provide. However, the bandwidth over the tuning range increases as tuning frequency goes up, since the real coupling between the parallel-coupled lines is frequency-dependent (proportional bandwidth tunable filter).

Alternatively, a ferromagnetic substrate, permeability (μ) is changed by DC biasing magnetic fields, can be used to tune the resonance frequency electronically [33]. Common techniques utilize ferromagnetic YIG resonators or ferrite slabs in resonators. When the ferroelectric slab is inserted at waveguide in the E-plane wall, the center frequency of the filter can be tuned [37].

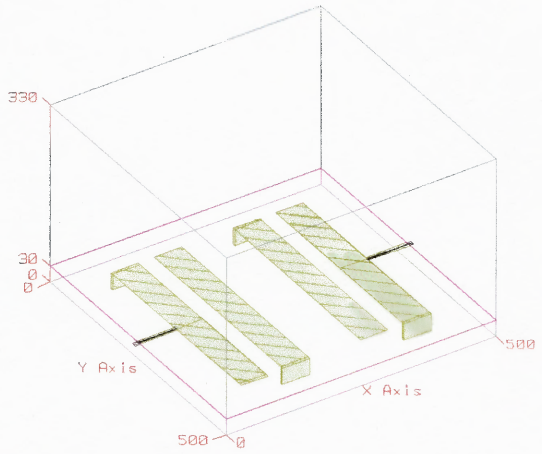

Figure 4.3 Four-pole tunable interdigital filter geometry.

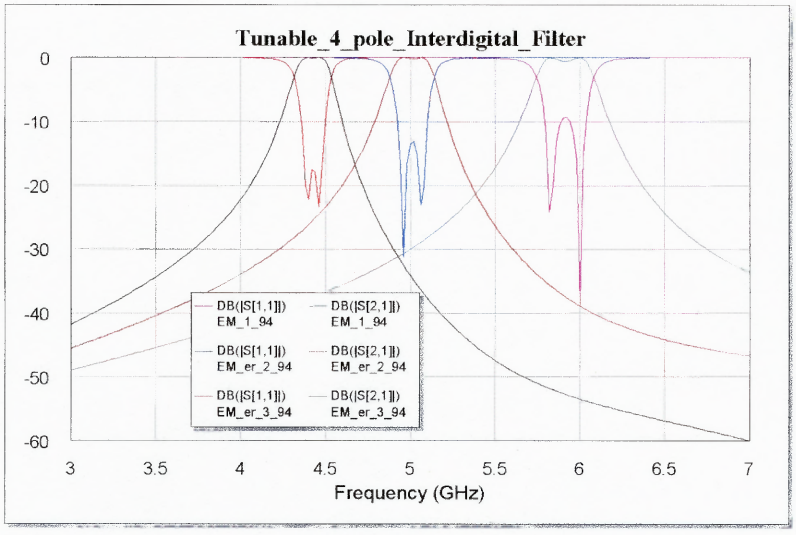

Figure 4.4 Filter response of the tunable filter; $\varepsilon_r = 1.94 \sim 3.94$.

It is desired to maintain constant bandwidth and response shape as the filter is tuned (absolute bandwidth tunable filter). When a stepped E-plane garnet slab is applied to evanescent waveguide filter design, the variation of the bandwidth over the tuning range can be compensated [38]. The ferrite slab thickness in the resonator region and coupling region is different in such an approach. A similar method can also be applied to

the microstrip filter design. Instead of the continuous ferroelectric substrate, inhomogeneous substrates can be used as tuning materials. Figure 4.5 shows a inhomogeneous substrate case, whereas Figure 4.7 shows stepped substrate case. Computer-analyzed results show that tuning range of the inhomogeneous substrates (Figure 4.6) is narrower than that of the stepped substrate case (Figure 4.8). When only substrates under the metal strip lines are tunable, the tuning range is approximately 20 percentage of the center frequency. For that amount of bandwidth, frequency-variable couplings are slightly varied over entire tuning range. Thus, bandwidth of an inhomogeneous substrate case is closer to the absolute bandwidth tunable filter.

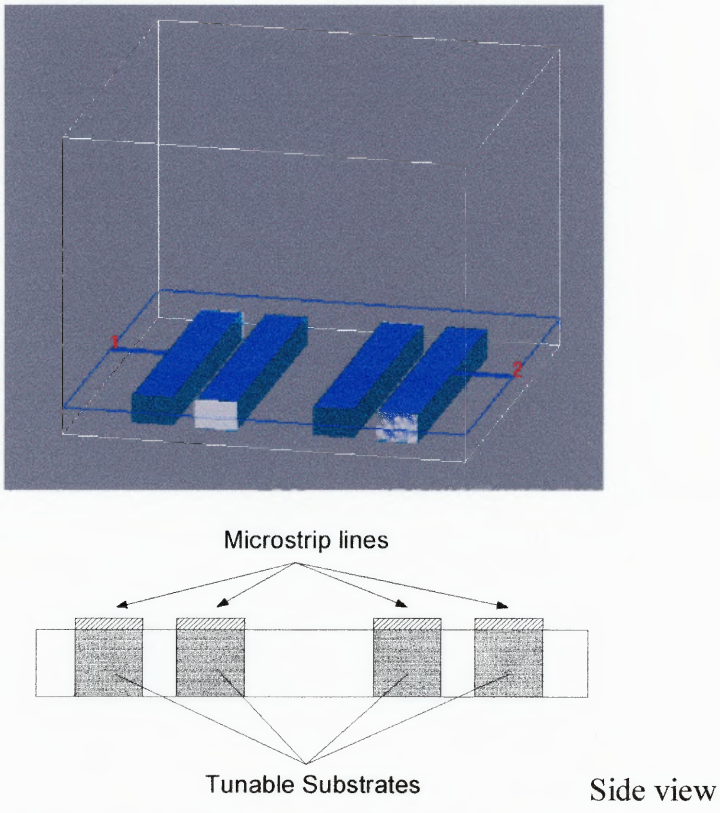

Figure 4.5 A tunable filter with inhomogeneous stripline substrates.

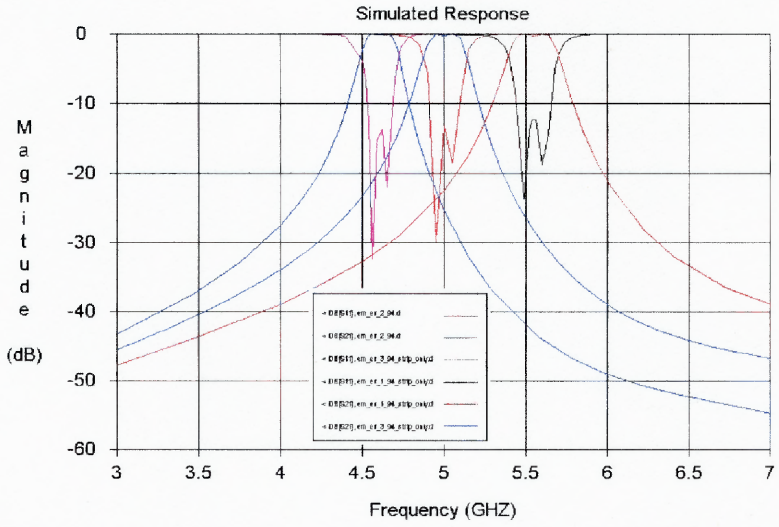

Figure 4.6 Filter response of the inhomogeneous substrate tunable filter; (ε_r: 1.94 ~ 3.94).

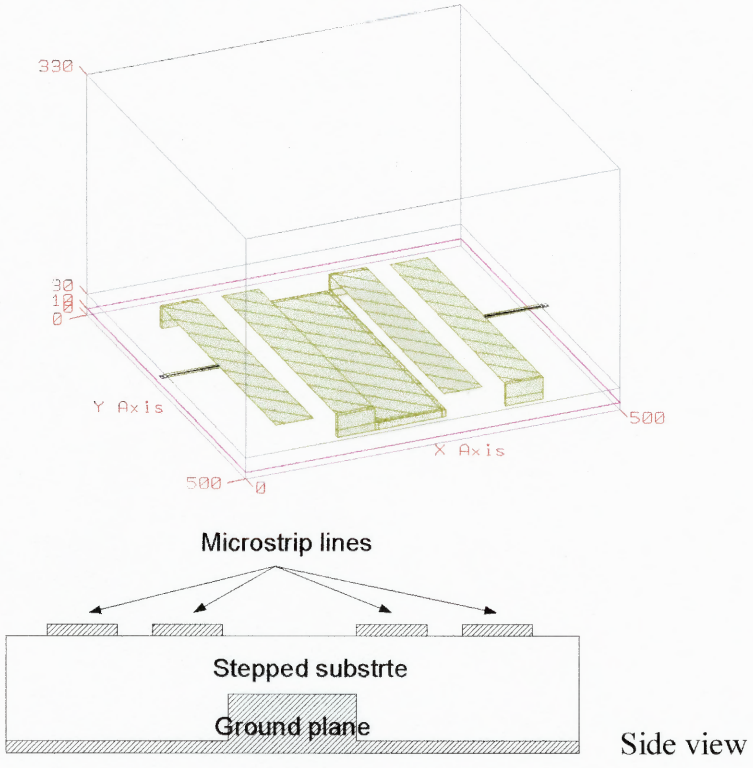

Figure 4.7 Four-pole tunable interdigital filter with a stepped ferroelectric substrate.

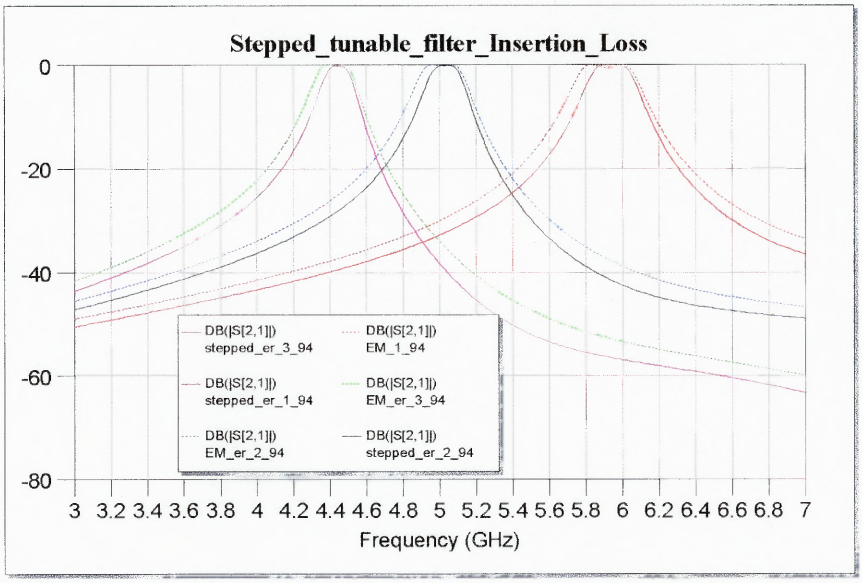

(a) Insertion Loss

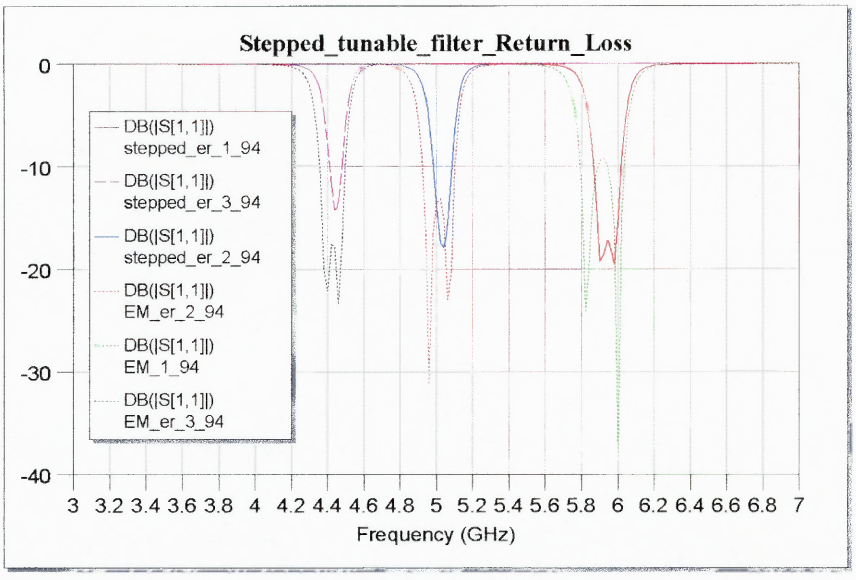

(b) Return Loss

Figure 4.8 Filter response of the four-pole tunable filter. (Solide line- steppd ferroelectric substrate, dotted line- continuous ferroelectric substrate.

However, both cases do not fully compensate the bandwidth variation in this simulation. Especially, for four-pole stepped interdigital filter, steps should be located between all PCL lines with different heights of steps. In order to simplify the tuning structure, a three-pole interdigital filter is considered as shown in Figure 4.9. In this approach, two different tunable substrates are used. One layer is the main substrate to tune the center frequency; the other layer is located between the PCL lines with the same height to obtain the absolute bandwidth. Return losses are not same at each end of the tuning range, since input-output impedance transformers are designed to the center frequency of the tuning range (Figure 4.10(a)). However, the bandwidth at each tuning stage is improved to meet the constant bandwidth (Figure 4.10(b)). This absolute bandwidth work is still in progress but shows possibilities.

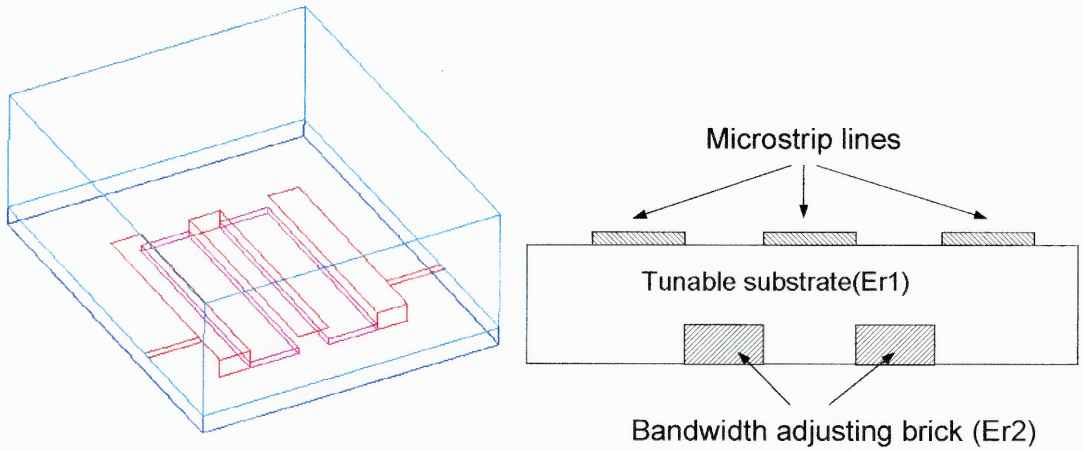

(a) 3-D geometry (b) Side view

Figure 4.9 Three-pole tunable interdigital filter.

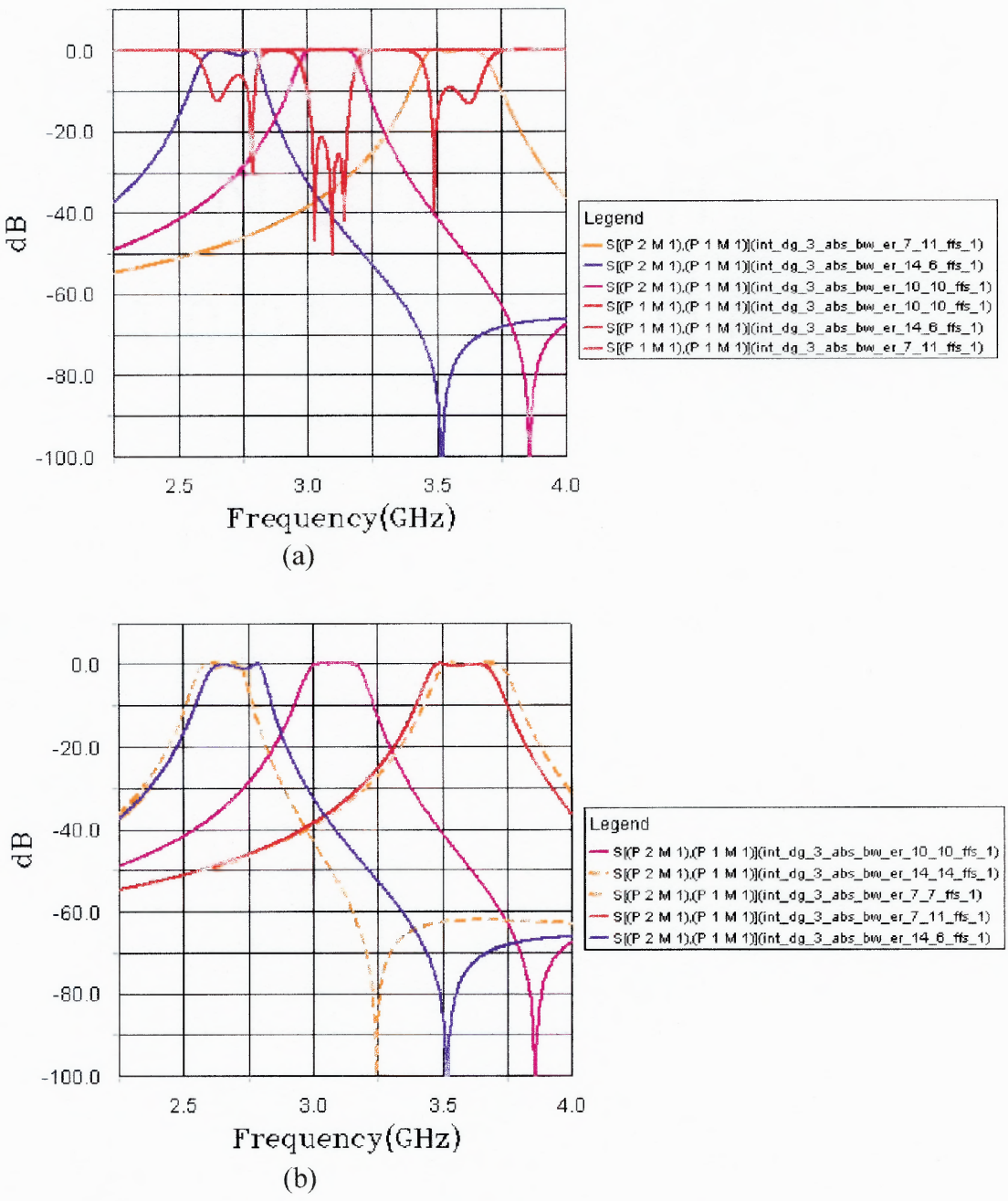

Figure 4.10 Tunable filter response of a three-pole interdigital filter; (a) Insertion and return loss at each tuning frequency, (b) Insertion loss comparison (Solid line- two tunable substrate case, dotted line- homogenous tunable substrate).

4.3 Transmission Zero Tunable Filter

Finite transmission zeros (FTZs) can be tuned to eliminate unwanted signals in the stopband by controlling of the cross-coupled network. Quasi-elliptic filters or generalized Chebychev filters can be synthesized without the cross-coupled networks. However, it is not easy to tune the FTZs only of the bandpass filter without affecting the original filter response. The circuit, which makes FTZs appear in the filter response, is also a part of the coupling network in the filter. In general, even-order bandpass filters which have the source-load coupling, contain the symmetrical transmission zeros. When these filters are cascaded through the proper coupling networks, each FTZs can be tuned independently.

A two-pole bandpass filter as shown in Figure 4.11 (a) is cascaded using a shunt capacitor between stages(Figure 4.11 (b)). Each two-pole bandpass filter has the source-load bridging capacitors. When one of the bridging capacitors is changed from the 0.1 pF to 0.001 pF, one pair of FTZs can be tuned. Two FTZs are located at the same frequency as an initial stage, since each bridging capacitor has the same capacitance (Figure 4.12(a)). After changing one bridging capacitor value, buried FTZs are separated and tuned independently (Figure 4.12 (b) ~ (e)). One pair of FTZs is kept to increase the selectivity of filter, and the other pair of FTZs is tuned to suppress variable unwanted signals in the stopband with keeping the original passband response. In order to realize tunable capacitance, a ferroelectric substrate can be considered as a substrate of bridging capacitor. Alternatively, ferromagnetic material also can be applied to make a variable inductive coupling circuit. Both case can serve as the solution to the high power tunable FTZ filter.

This cross-coupled two-pole filter can be employed to place FTZs symmetrically or asymmetrically in the stopband. When these filters are used as input-output stages, this method can be easily extended to higher order filter. As for the high power application, a ferromagnetic material, such as Garnet, can be considered for the cross-coupling tuning circuit.

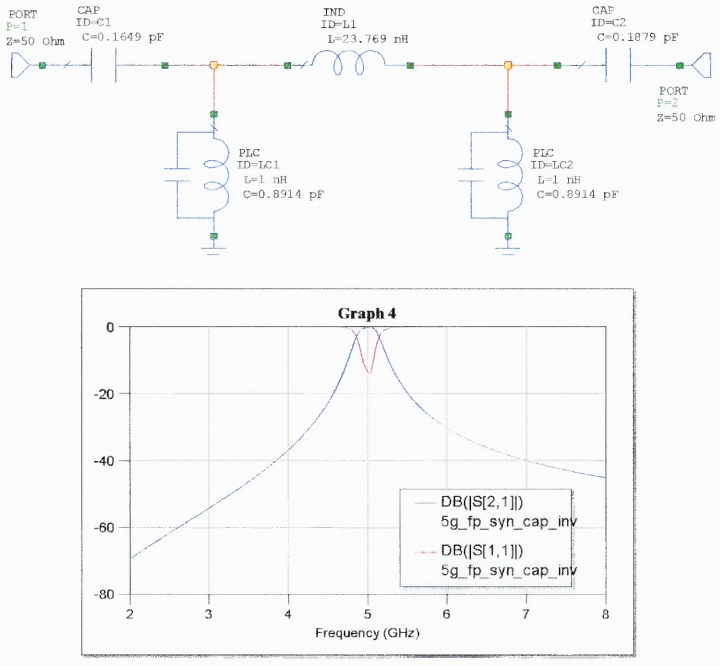

(a) two-pole subcircuit filter and response

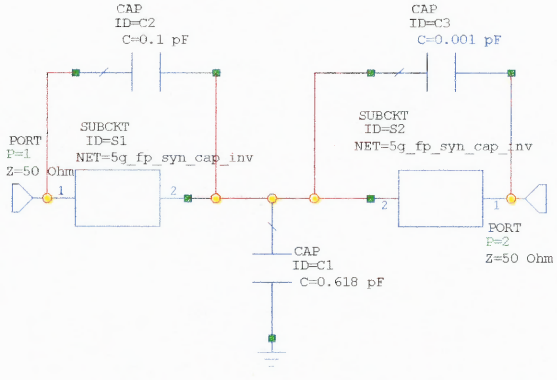

(b) four pole filter with the bridge capacitors

Figure 4.11 Cascaded four-pole filter.

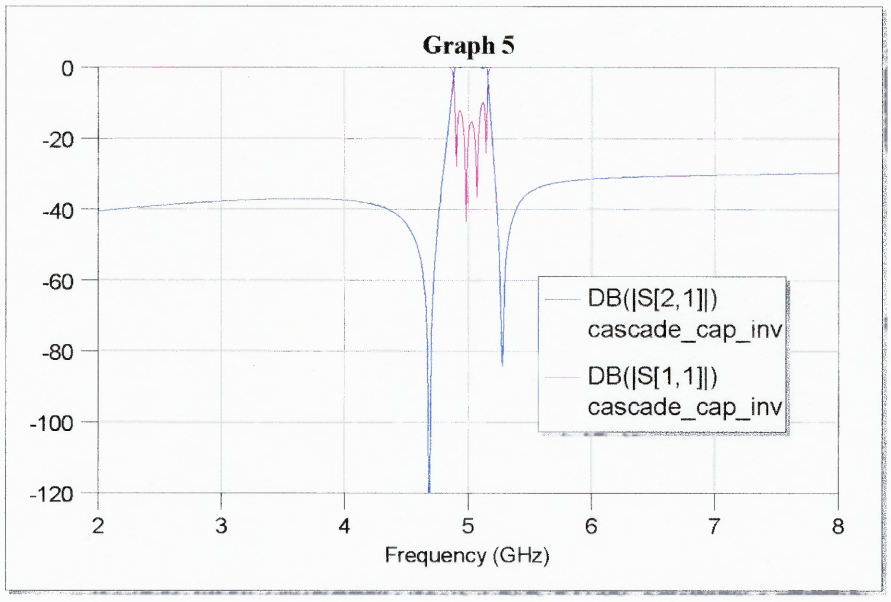

(a) C3 =0.1 pF

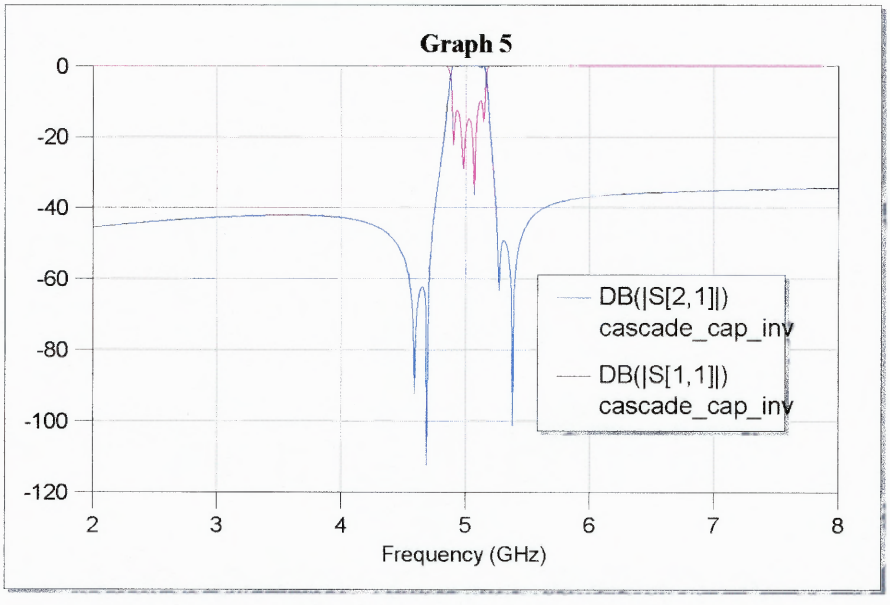

(b) C3 = 0.05 pF

Figure 4.12 TZs tuned by changing a bridging capacitor.

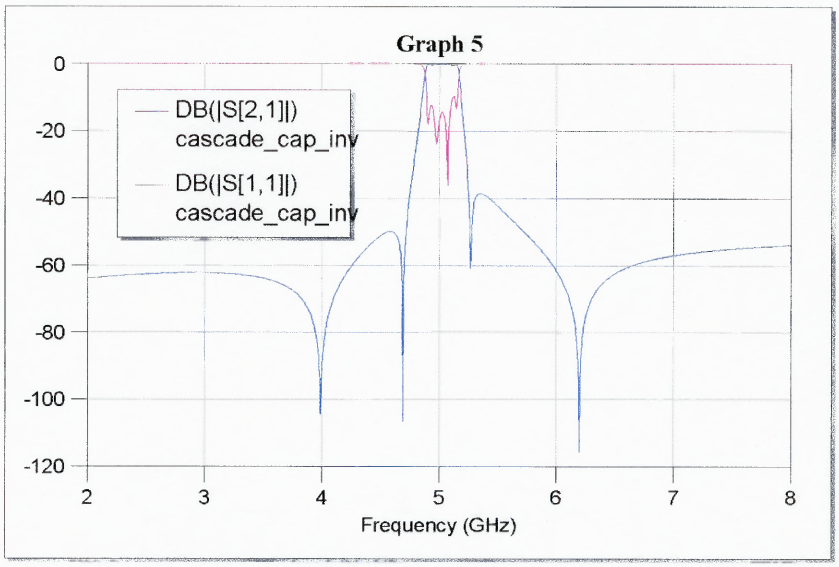

(c) C3= 0.006 pF

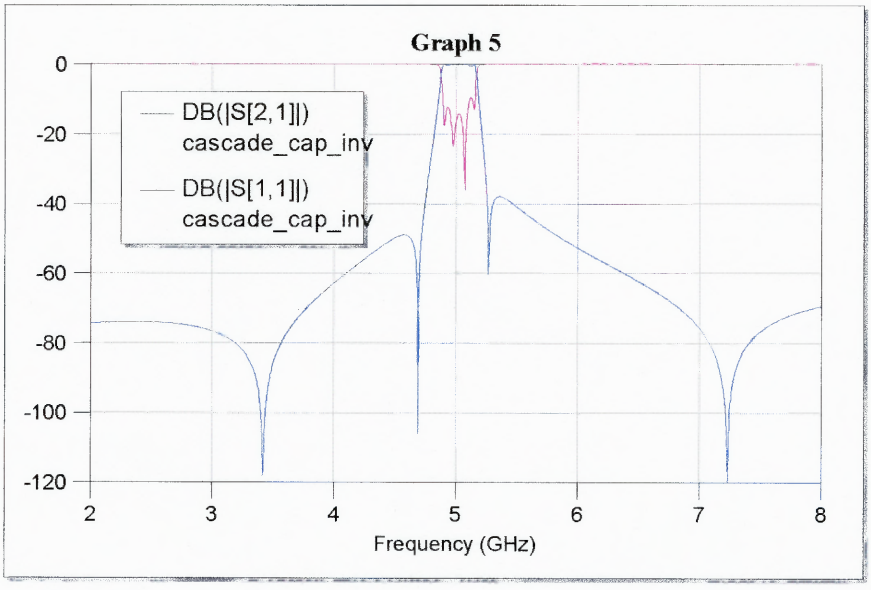

(d) C3 = 0.002 pF

Figure 4.12 TZs tuned by changing a bridging capacitor (contined).

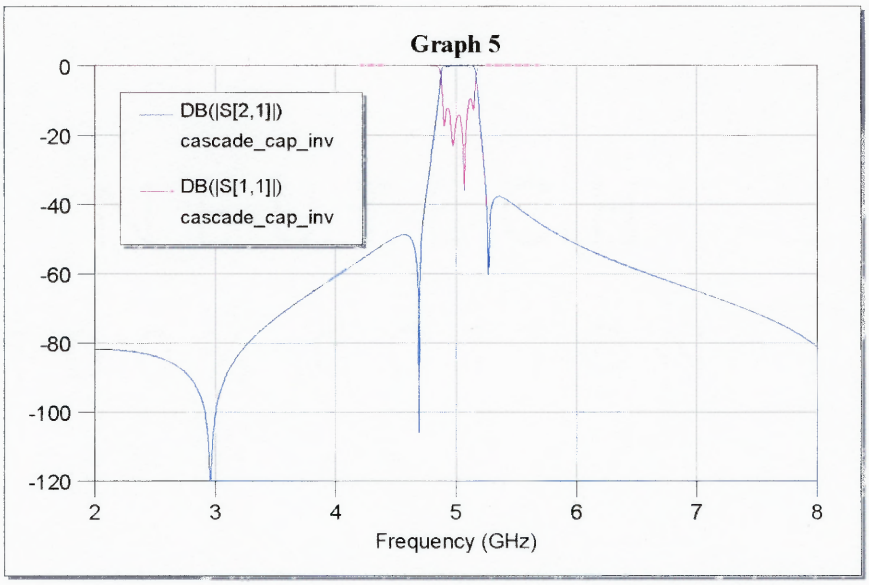

(e) C3 = 0.001pF.

Figure 4.12 TZs tuned by changing a bridging capacitor (contined).

4.4 Conclusions

In this chapter, conventional tunable filter design methods have been applied to the interdigital filter structure. A frequency-independent coupling tunable filter was proposed, and a technique was demonstrated to implement the required coupling coefficients over the tuning range. A stepped or inhomogeneous substrate interdigital filter was proposed as bandwidth compensation techniques. Finally, a new concept of the transmission-zero tunable filter was presented using a cascaded cross-coupled coupler with a tunable substrate.

CHAPTER 5

CONCLUSIONS AND FUTURE WORK

In this dissertation, various methods were explored to locate the transmission zeros on the complex frequency domain efficiently, which improve the filter selectivity or flatten the group delay.

Quasi-elliptic combline filters with a new type of cross-coupled network were considered in Chapter 1. The responses of each filter were presented by using circuit, full E-M simulator, and pole-zero locator program. An open-circuited PCL combline filter showed the negative coupling effect which is not be available in the conventional combline filter. A distributed top surface-metalized transmission line coupler was used to implement the source-load direct coupling and consequent extra TZs.

In the second chapter, the use of tunable quasi-elliptic short-terminated combline filters (STCL) as matched reactive loads on a 90-degree hybrid coupler was shown to provide double the insertion phase of each filter. The overall insertion loss is lower, and phases shift range greater than with the conventional L-C approaches. A two-pole quasi-elliptic combline pair has been shown to asymptotically approach 360-degree total phase shift, with a large linear range and an insertion loss of less than -1.5 dB over the full phase shift range. Extension to higher order combline or other coupled line networks should easily extend the phase shift range well beyond 360 degrees, and combline structures are practical at both higher and lower frequencies.

The third chapter examined the difference between the filter response computed assuming frequency invariable couplings and the real response based on real frequency - variable couplings. An efficient top surface-metalized dielectric "brick" overlay to be

used in the planar bandpass filter design, was presented for the source-load cross coupling as a frequency dependent coupling. Two cross-coupled networks were cascaded as basic filter elements such as CT or CQ resonators to improve filter responses.

In Chapter 4, a new concept of tunable filters was considered. The classical tunable filter design methods, including ferromagnetic and ferroelectric substrate, were applied to the microstrip filter structure. The tunable TZ filter was proposed to be used for rejecting variable unwanted signals, with potential application to high power transmitters.

A variety of cross coupling methods have been proposed from the negative coupling effects of the open-circuit parallel coupled combline filter to the tunable TZ filter. Future work will focus on the high power tunable filter implementation using real ferroelectric and ferromagnetic substrates.

APPENDIX

POLE-ZERO LOCATOR PROGRAM

These programs are Matlab source code of the pole-zero locator program.

1) Main function : y_trans.m

```
% Pole-zero locator and circuit analysis program
% y_trans.m
% 09/18/01
%
% By Sanghoon Shin
% NJIT
% ECE Department
% Microwave Laboratory

function y_trans(fn)
close all

[y,dim,Zg] = read_data(fn); % input data function call

syms s
Zo=Zg;

%frequency setup
%%%%%%%%%%%%%%%%%%%%
fs = 1e9; %frequency scaling factor
f1=1; %plot start frequency
f2=8; %plot stop frequency
step=401; % number of frequency steps

cur = zeros(1,dim); % current column vector
cur(1,1)=1;
cur = cur';

v = y\cur; % calculate node voltages
transf = 1/Zo*v(dim); % calculate transfer function

[n,d] = numden(transf);
zc = sym2poly(n); % generate numerator polynomials
pc = sym2poly(d); % generate denominator polynomials

zeros=roots(zc) % call root finding routine
poles=roots(pc)

Ys=1/Zo;

%w = linspace(0,2,201)*fs; % frequency in radian
f = linspace(f1,f2,step)*fs; % frequency in Hz

s21=2*Ys*v(dim); % Calculate Insertion Loss
s21_num=subs(s21,s,j*2*pi*f); % freq.  in Hz
```

```
IR_db = 20*log10(abs(s21_num));

grid
gamma_in=2*v(1)*Ys-1;
RL=subs(gamma_in,s,j*2*pi*f); % Calculate Return Loss
RL_db = 20*log10(abs(RL));

% Plot routine
%%%%%%%%%%%%%%%%%%%%%%%%%%%%%%%%%%%%%%%%%%%%%%%%%%%%5
subplot(1,2,1)
plot(poles/(2*pi),'rx') % plot in Hz
hold on
plot(zeros/(2*pi),'bo')
xlabel('Real Axis')
ylabel('Imaginary Axis')
axis([-4 0 f1 f2]*fs)
title('Pole-Zero plot')
grid

subplot(1,2,2)
plot(IR_db,f,'-r') % frequency in Hz
hold on
plot(RL_db,f,'-.b')
set(gca,'XDir','reverse')
legend('IR(S21)','RL(S11)',0)
title('Magnitude')
ylabel('Frequency {\itf}, GHz');
xlabel('IL,RL (dB)');
box off
grid

figure
plot(f,IR_db,'-r',f,RL_db,'-.b') % frequency in Hz
legend('IR(S21)','RL(S11)',0)
title('Magnitude')
xlabel('Frequency {\itf}, GHz');
ylabel('IL,RL (dB)');
grid

%Plot polz-zero

figure
plot(poles/(2*pi),'rx') % plot in Hz
hold on
plot(zeros/(2*pi),'bo')
%axis([-1 0 f1 f2]*fs)
title('pole-zero plot')
axis equal
grid

zeros=zeros/(2*pi)
poles=poles/(2*pi)

figure
subplot(2,1,1)
```

```
plot(f,IR_db)
grid

% Phase response Plot
subplot(2,1,2)
plot(f,angle(s21_num))
ylabel('phase')
grid
%%%%%%%%%%%%%%%%%%%%%%%%%%%%%%%%%%%%%%%%%%%%%%%%
```

2) Input Matlab function routine for the spice format data : read_data.m

```
% read_data.m
% Input function for spice format
% 09/12/01
% By Sanghoon Shin
% NJIT
% ECE Department
% Microwave Laboratory

fid = fopen( 'data_test.txt', 'r' ); % to check m-matrix

m = fscanf( fid,'%s %i %i %f %f', [5, inf] );

mx = max(m');
mx2 = max( mx(2:3) );

syms s;
mat = sym( zeros( mx2, mx2 ) );

[ nr nc ] = size(m);

for col = [1:1:nc]

   d = m(:,col);

   if d(1) == 114 | d(1) == 82   % R : register
      if d(3) == 0
         mat ( d(2), d(2) ) = mat (d(2),d(2)) + 1/d(4);
      else
         d(2) < d(3)
         mat ( d(2),d(3)) = mat (d(2),d(3)) - 1/d(4);
         mat ( d(2),d(2)) = mat (d(2),d(2)) + 1/d(4);
         mat ( d(3),d(3)) = mat (d(3),d(3)) + 1/d(4);
      end

   elseif d(1) == 99 | d(1) == 67 % C : capcitor
      if d(3) == 0
         mat ( d(2), d(2) ) = mat (d(2), d(2)) + sym(s*d(4));
      else
         d(2) < d(3)
         mat ( d(2),d(3)) = mat (d(2),d(3)) - sym(s*d(4));
         mat ( d(2),d(2)) = mat (d(2),d(2)) + sym(s*d(4));
```

```
         mat ( d(3),d(3)) = mat (d(3),d(3)) + sym(s*d(4));
      end

   elseif d(108) % L ; inductor
      if d(3) == 0
         mat ( d(2), d(2) ) = mat (d(2), d(2)) + sym(s/d(4));
      else
         d(2) < d(3)
         mat ( d(2),d(3)) = mat (d(2),d(3)) - sym(1/(s*d(4)));
         mat ( d(2),d(2)) = mat (d(2),d(2)) + sym(1/(s*d(4)));
         mat ( d(3),d(3)) = mat (d(3),d(3)) + sym(1/(s*d(4)));
      end
   end

   else d(1) == 112  % P: shunt parallel LC tank circuit
      if d(3) == 0
         mat ( d(2), d(2) ) = mat (d(2), d(2)) +
sym(1/(s*d(4))+s*d(5));
      else
         d(2) < d(3)
         mat ( d(2),d(3)) = mat (d(2),d(3)) - sym(1/(s*d(4))+s*d(5));
         mat ( d(2),d(2)) = mat (d(2),d(2)) + sym(1/(s*d(4))+s*d(5));
         mat ( d(3),d(3)) = mat (d(3),d(3)) + sym(1/(s*d(4))+s*d(5));
      end

   end

end

%to make symmetric matrix
for col = [2:1:mx2]
   for row = [1:1:col]
      mat( col, row ) = mat( row, col );
   end
end

fclose(fid);
```

3) Input data example: four-pole bandpass filter with a source-load bridging capacitor

bpf4_5g_cross.txt

R 1 0 50 0
P 1 0 0.0593e-9 17.646e-12
L 1 2 1.7046e-9 0
P 2 0 0.0593e-9 18.12e-12
L 2 3 2.1258e-9 0
P 3 0 0.0593e-9 18.12e-12
L 3 4 1.7046e-9 0
P 4 0 0.0593e-9 17.646e-12
C 1 4 0.0413e-12 0
R 4 0 50 0

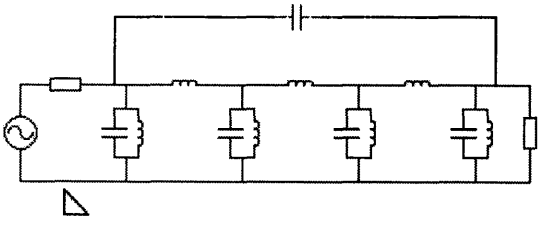

Usage: At the Matlab command window, type in followings

>>Matlab> y_trans('bpf4_5g_cross.txt')

Results:

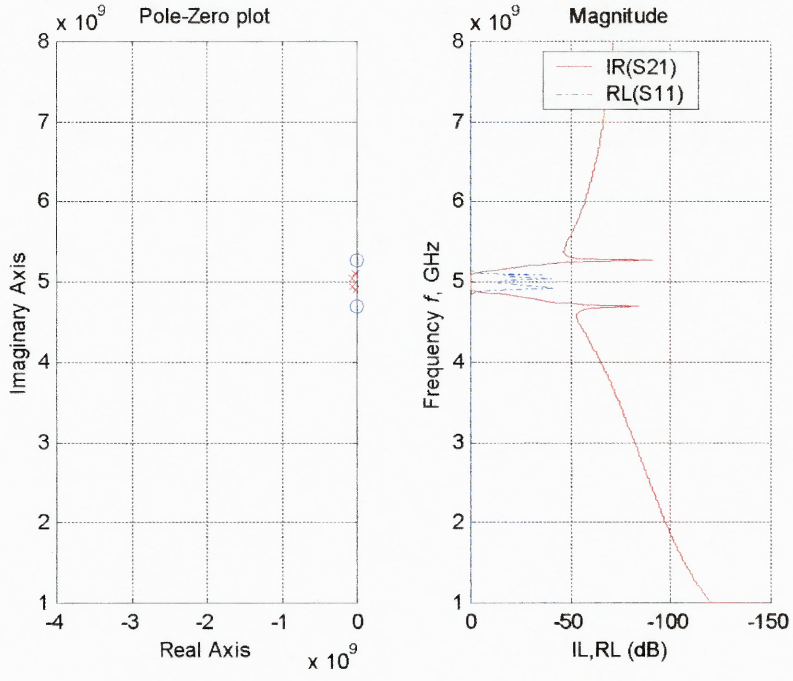

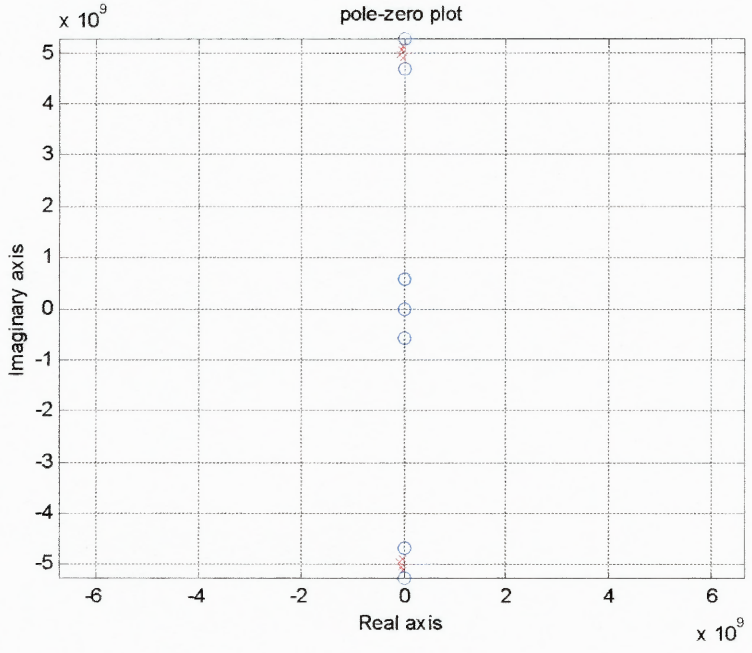

REFERENCES

1. S. Hong and M.J. Lancaster, "Couplings of Microstrip Square Open-Loop Resonator for Cross-Coupled Planar Microwave Filters," 1996 Transactions on Microwave Theory and Techniques 44.11 (Nov. 1996 [T-MTT]): pp. 2099-2109.

2. Ralph Levy and S.B. Cohn, "A History of Microwave Filter Research, Design, and Development," 1984 Transactions on Microwave Theory and Techniques (Sep. 1984 [T -MTT] (Special Centennial Issue Historical Perspectives of Microwave Technology)): pp. 1055-1067.

3. I. C. Hunter and J.D. Rhodes, "Electronically Tunable Microwave Bandpass Filters," Transactions on Microwave Theory and Techniques 30.9 (Sep. 1982 [T-MTT] (Special Issue on Microwave Filters)), pp. 1354-1360.

4. R.M. Kurzrok, "Design of Comb-Line Band-Pass Filters (Correspondence)," 1966 Transactions on Microwave Theory and Techniques 14.7 (Jul. 1966 [T-MTT]): pp. 351-353.

5. G. L. Matthaei, L. Young, and E.M.T. Jones, "Microwave Filter, Impedance-Matching Network, and Coupling Structures," McGraw-Hill, 1964.

6. Richard V. Snyder, "Inverted-Resonator Evanescent Mode Filters," 1996 MTT-S International Microwave Symposium Digest 96.2 (1996 Vol. II [MWSYM]): pp. 465-468.

7. Y.S. Lee, "Mode Compensation Applied to Parallel-Coupled Microstrip Directional Filter Design," 1974 Transactions on Microwave Theory and Techniques 22.1 (Jan.1974 [T -MTT]), pp. 66-69.

8. Smain Amri, "Direct Synthesis of Folded Symmetric Resonator Filters with Source-Load Coupling," 2001 IEEE Microwave and wireless Components Letters, Vol. 11, No. 6, June 2001; pp. 264-266.

9. J.R. Montejo-Garai, "Synthesis of N-even order symmetric filters with N transmission zeros by means of source-load cross coupling," IEEE Electronics Letters February 2000, Vol. 36 No. 3.

10. Agilent Technology, "Network Analysis Solutions Advanced Filter Tuning Using Time Domain Transforms (AN 1287-10)".

11. Chi Wang and Kawthar A. Zaki, "Temperature Compensation of Combline Resonators and Filters," 1999 IEEE MTT-S Int. Microwave Symposium Digest, Vol. 3, pp.1041 -1044, 1999.

12. Uysal, "Nonuniform Line Microstrip Directional Couplers and Filters," Vol. II, Boston, MA: Artech House, 1993.

13. Shiban K. Koul Bharathi Bhat, "Microwave and Millimeter Wave Phase Shifter," Vol. II, MA: Artech House, 1991.

14. Peter Shveshkeyev, "A Varactor Controlled Phase Shifter for PCS Base Station Applications," Microwave Product Digest, June 2000.

15. S. R. Chandler, "Active Varactor Tunable Bandpass Filter," IEEE Microwave and Guided Letters, Vol.3, pp. 70 - 71, March 1993.

16. Richard V. Snyder, "The RF and Microwave Handbook," Chapter 5.9, CRC Press, 2000.

17. Yoshihisa Amano, Atsushi Yamada, Eiji Suematsu and Hiroya Sato, " A Low Cost Planar Filter For 60 GHz applications," Microwave Journal, March 2001.

18. Agilent Technologies, "Advanced Design System Ver. 1.3," 1999.

19. N. Yildirim, "Filpro Manual," METU, Ankara, Turkey, November 1996.

20. Sanghoon Shin, Richard V. Snyder, Edip Niver, "360-degree Linear Analog Phase Shifter Design Using Tunable Short-circuit Terminated Combline Filters," 2001 IEEE MTT-S Int. Microwave Symposium Digest Vol. 1, pp. 303 – 306, 2001.

21. Richard J. Cameron, "General Coupling Matrix Synthesis Methods for Chebyshev Filtering Functions," IEEE Transactions Microwave Theory and Technique, Vol. 47, No. 4, April 1999.

22. H. Clark Bell, JR, "Canonical Asymmetric Coupled-Resonator Filters," IEEE Transactions on Microwave Theory and Technique, Vol. MTT-30, No.9 Sep., 1982.

23. Ali E. Atia, Albert E. Williams, "Narrow-Bandpass Waveguide Filters," IEEE Transactions on Microwave Theory and Technique, Vol. MTT-20, No.4 Sep., 1972.

24. Ralph Levy, "Direct Synthesis of Cascaded Quadruplet (CQ) Filters," IEEE Transactions on Microwave Theory and Techniques, Vol. 43, No. 12, Dec. 1995.

25. Smain Amari, "On the Maximum Number of Finite Transmission zeros of coupled resonator filters with a given topology," IEEE Microwave and Guided wave Letters, Vol. 9, No. 9, Sep. 1999.

26. Smain Amari, "Direct synthesis of Folded symmetric resonator filters with source-load coupling," IEEE Microwave and wireless components letters, Vol. 11, No. 6, June 2001.

27. Smain Amari, J. Boremann, "Using Frequency-Dependent Coupling to Generate Finite Attenuation Poles in Direct-coupled Resonator Bandpass Filters," IEEE Microwave and Guided Wave Letters, Vol. 9, No. 10, Oct 1999.

28. W. A. Atia, Kawthar A. Zaki, Ali E. Atia, "Synthesis of general topology multiple coupled resonator filters by optimization," IEEE Microwave Theory Tech. Dig. pp. 821-824, 1998.

29. Smain Amari, "Synthesis of Cross-Coupled Resonator Filters Using an Analytical Gradient-Based Optimization Technique," IEEE Transactions and Microwave Theory and Techniques, VOL.48, No. 9, Sep., 2000.

30. Richard V. Snyder, "Synthesis of Filters with Frequency Variable Couplings (FVC)," IEEE International Microwave Symposium Workshop, May 2001.

31. G.L. Matthaei, L. Young, E.M.T. Jones, "Microwave Filters, Impedance-Matching Networks, and Coupling Structures", New York, McGraw-Hill, Ch. 17, 1964.

32. Chi-Yang Chang, Tastsuo Itoh, "A Varactor-tuned, active microwave band-pass filter," IEEE MTT-s, Vol. MWSYM, 1999, pp. 499 - 502.

33. R.R. Jones, J. Cunningham and K. Bulllock, "Magnetically Tunable Microstrip Filter Structures," IEEE 1968 MWSYM, pp. 282-290.

34. H. Kim, J. Park, Y. Kim,and Y. Kwon, "Millimeter-wave Micromachined Tunable Filters," 1999 MTT-s International Microwave Symposium Digest Vol.3, 1235-1238.

35. G. Subramnayam, Fred Keuls, Felix Miranda, "A K-band Tunable Microstrip Bandpass filter Using a thin-film conductor/ferroelectric/dielectric multilayer configuration," IEEE Microwave and guided wave letters, Vol. 8. No.2, Feb, 1998.

36. Jaroslaw Uher, J. Bornemann, F. Arndt, "Ferrite tunable millimeter wave printed circuit filters," IEEE MTT-S Digest, 1988.

37. D.E. Oates and G.F. Dionne, "Tunable superconducting resonators using Ferrite substrate," 1997 MTT-s International Microwave Symposium Digest Vol.1, pp. 303-306.

38. Richard V. Snyder, "Stepped-Ferrite Tunable Evanescent filters," IEEE Transactions on Microwave and Techniques, Vol. MTT-29, Vol.29, April 1981.

39. Ian Hunter, "The Theory and Design of Microwave filters," IEE Electromagnetic waves series 48, pp. 263-266, 2001.

40. Sanghoon Shin, Richard V. Snyder, "At least N+1 Finite Transmission Zeros Using Frequency Dependent Negative Source-load Coupling," Microwave and Wireless components letters, submitted March 2002.

41. I. C. Hunter and John David Rhodes, "Electronically Tunable Microwave Bandpass Filters," IEEE Transactions on Microwave Theory and Techniques, Vol., MTT-30, No. 9, Sep. 1982.

42. George F. Craven, Richard F. Skedd, "Evanescent Mode Microwave Components," Artech House, 1987.